Coupling of Neural Computation with Physical Computation for Stable Dynamic Biped Walking Control

Tao Geng[1], **Bernd Porr**[2] **Florentin Wörgötter**[1,3]

[1]Department of Psychology, University of Stirling, Stirling, UK
[2]Department of Electronics & Electrical Engineering, University of Glasgow, UK
[3]Bernstein Center for Computational Neuroscience, University of Göttingen, Germany

Abstract

Biped walking remains a difficult problem and robot models can greatly facilitate our understanding of the underlying biomechanical principles as well as their neuronal control. The goal of this study is to specifically demonstrate that stable biped walking can be achieved by combining the physical properties of the walking robot with a small, reflex based neuronal network, which is governed mainly by local sensor signals. Building on earlier work (Taga, 1995; Cruse et al., 1998), this study shows that human-like gaits emerge without specific position or trajectory control and that the walker is able to compensate small disturbances through its own dynamical properties. The reflexive controller used here has the following characteristics, which are different from earlier approaches: (1) Control is mainly local. Hence, it uses only two signals (AEA=Anterior Extreme Angle and GC=Ground Contact) which operate at the inter-joint level. All other signals operate only at single joints. (2) Neither position control nor trajectory tracking control is used. Instead, the approximate nature of the local reflexes on each joint allows the robot mechanics itself (e.g., its passive dynamics) to contribute substantially to the overall gait trajectory computation. (3) The motor control scheme used in the local reflexes of our robot is more straightforward and has more biological plausibility than that of other robots, because the outputs of the motor-neurons in our reflexive controller are directly driving the motors of the joints, rather than working as references for position or velocity control. As a consequence, the neural controller and the robot mechanics are closely coupled as a neuro-mechanical system and this study emphasizes that dynamically stable biped walking gaits emerge from the coupling between neural computation and physical computation. This is demonstrated by different walking experiments using a real robot as well as by a Poincare map analysis applied on a model of the robot in order to assess its stability.

1 Introduction

There are two distinct schemes for leg coordination discussed in the literature on animal-locomotion and on biologically-inspired robotics, namely CPGs (Central Pattern Generators) and reflexive controllers. It was found that motor-neurons (and hence rhythmical movements) in many animals are

driven by central networks of inter-neurons that generate the essential features of the motor pattern. However, sensory feedback signals also play a crucial role in such control systems by turning a stereotyped unstable pattern into the co-coordinated rhythm of natural movement (Reeve, 1999). These networks were referred to as CPGs. On the other hand, Cruse developed a reflexive controller model to understand the locomotion control of a slowly-walking stick insect (Carausius morosus). In his model, reflexive mechanisms in each leg generate the step cycle of each individual leg. For inter-leg coordination, in accordance to observations in insects, he presented six mechanisms that can re-establish coordination in the case of minor disturbances (Cruse et al., 1998; Cruse and Warnecke, 1992).

While neural systems modeled as CPGs or reflexive controllers explicitly or implicitly compute walking gaits, the mechanics also "compute" a large part of the walking movements (Lewis, 2001). This is called physical computation, namely exploiting the system's physics, rather than explicit models, for global trajectory generation and control. One distinct example of physical computation in animal locomotion is the "preflex"; the nonlinear, passive visco-elastic properties of the musculoskeletal system itself (Brown and Loeb, 1999). Due to the physical nature of the preflex, the system can respond rapidly to disturbances (Cham et al., 2000). Thus, in all animals locomotion control is shared between neural computation and physical computation.

In the current work, we present our design of a novel reflexive neural controller that has been implemented on a planar biped robot. We will show how a dynamically stable biped walking gait emerges on our robot as a result of a combination of neural- and physical computation. Several issues are addressed in this paper which we believe are of relevance for the understanding of biologically motivated walking control. Specifically we will show that it is possible to design a walking robot with a very sparse set of input signals and with a controller that operates in an approximate and self-regulating way. Both aspects may be of importance in biological systems too, because they allow for a much more limited structure of the neural network and reduce the complexity of the required information processing. Furthermore, in our robot the controller is directly linked to the robot's motors (its "muscles") leading to a more realistic, reflexive sensor-motor coupling than implemented in related approaches. These mechanisms allowed us for the first time to arrive at a dynamically stable artificial biped combining physical computation with a pure reflexive controller.

The experimental part of this study is complemented by a dynamical model and the assessment of its stability using a Poincare map approach. Robot simulations have been recently criticised, raising the issue that complex systems, like a walking robot, cannot be fully simulated because of uncontrollable contingencies in the design and in the world in which it is embedded. This notion, known as the "embodiment problem" has been discussed to a large extent in the robotics literature in the last years (Porr and Wörgötter, 2005; Ziemke, 2001). This issue reappears also in our case where we find that the simulations and their analysis will indeed match the experiments and raise confidence in the design, while stopping short of the rich detail of the real system.

This paper is organized as follows. First we describe the mechanical design of our biped robot. Next, we present our neural model of a reflexive network for walking control. Then we demonstrate the result of several biped walking experiments and apply Poincare map analysis on the robot model. Finally, we compare our reflexive controller with other walking control mechanisms.

2 The robot

Reflexive controllers such as Cruse's model involve no central processing unit that demands information on the real-time state of every limb and computes the global trajectory explicitly. Instead, local reflexes of every limb require only very little information concerning the state of the other limbs. Coordinated locomotion emerges from the interaction between local reflexes and the ground. Thus, such a distributed structure can immensely decrease the computational burden of the locomotion controller. With these eminent advantages, Cruse's reflexive controller and its variants had been implemented on some multi-legged robots (Ferrell, 1995). Whereas in the case of biped robots, though some of them also exploit some form of reflexive mechanisms, their reflexes usually work as an auxiliary function or as infrastructural units for other non-reflexive high-level or parallel controllers. For example, on a simulated 3D biped robot (Boone and Hodgins, 1997), specifically designed reflexive mechanisms were used to respond to two types of ground surface contact errors of the robot, slipping and tripping, while the robot's hopping height, forward velocity, and body attitude are separately controlled by three decoupled conventional controllers. On a real biped robot (Funabashi et al.,

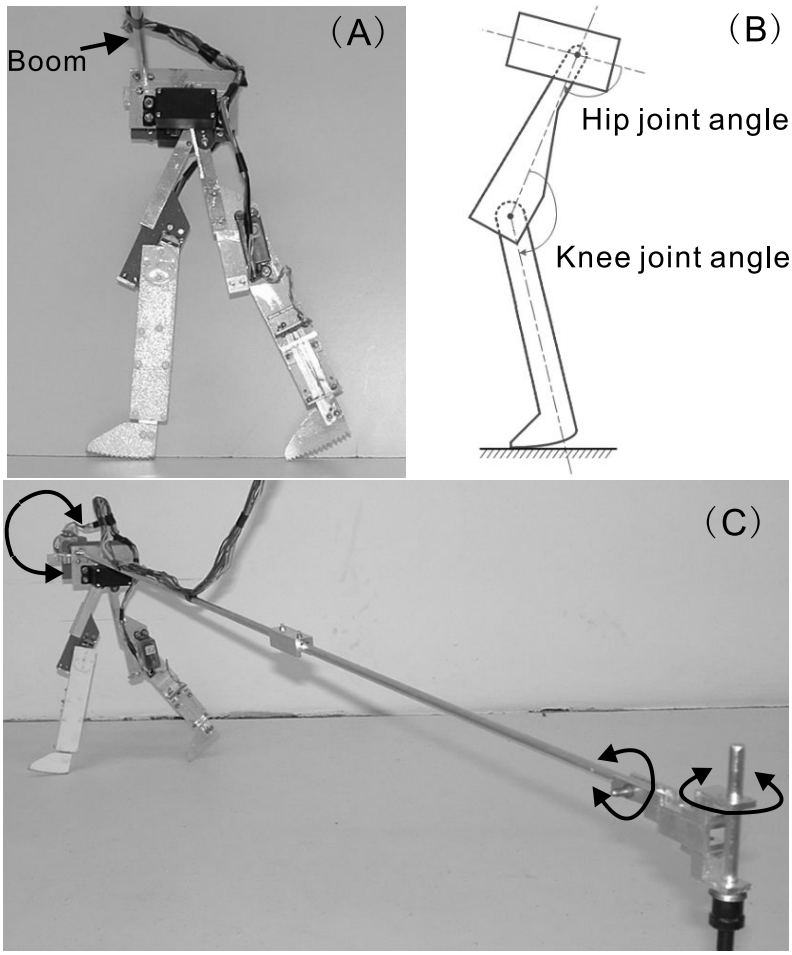

Figure 1: A) The robot and B) a schematic of the joint angles of one leg. C) The structure of the boom. All its three orthogonal axes (pitch, roll and yaw) rotate freely, thus having no influence on the robot dynamics in its saggittal plane.

2001), two pre-wired reflexes are implemented to compensate for two distinct types of disturbances representing an impulsive force and a continuous force, respectively. To date, no real biped robot has existed that depends exclusively on reflexive controllers for walking control. This may be because of the intrinsic instability specific to biped-walking, which makes the dynamic stability of biped robots much more difficult to control than that of multi-legged robots. After all, a pure local reflexive controller itself involves no

mechanisms to ensure the global stability of the biped.

While the controllers of biped walking robots generally require some kind of continuous position feedback for trajectory computation and stability control, some animals' fast locomotion is largely self-stabilized due to the passive, visco-elastic properties of their musculoskeletal system (Full and Tu, 1990). Not surprisingly, some robots can display a similar self-stabilization property (Iida and Pfeifer, 2004). Passive biped robots can walk down a shallow slope with no sensing, control, or actuation. However, compared with a powered biped, passive biped robots have obvious drawbacks, e.g., needing to walk down a slope and their inability to control speed (Pratt, 2000). Some researchers have proposed to equip a passive biped with actuators to improve its performance. Van der Linde made a biped robot walk on level ground by pumping energy into a passive machine at each step (Van der Linde, 1998). Nevertheless, no one has yet built a passive biped robot that has the capabilities of powered robots, such as walking at various speeds on various terrain (Pratt, 2000).

Passive biped robots are usually equipped with circular feet, which can increase the basin of attraction of stable walking gaits , and can make the motion of the stance leg look smoother. Instead, powered biped robots typically use flat feet so that their ankles can effectively apply torque to propel the robot to move forward in the stance phase, and to facilitate its stability control. Although our robot is a powered biped, it has no actuated ankle joints, rendering its stability control even more difficult than that of other powered bipeds. Since we intended to exploit our robot's passive dynamics during some stages of its gait cycle, similarly to the passive biped, its foot bottom also follows a curved form with a radius equal to the leg-length.

As for the mechanical design of our robot, it is 23 cm high, foot to hip. It has four joints: left hip, right hip, left knee, and right knee. Each joint is driven by an RC servo motor. A hard mechanical stop is installed on the knee joints, thus preventing the knee joint from going into hyperextension, similar to the function of knee caps on animals' legs. The built-in PWM (Pulse Width Modulation) control circuits of the RC motors are disconnected while its built-in potentiometer is used to measure joint angles. Its output voltage is sent to a PC through a DA/AD board (USB DUX, www.linux-usb-daq.co.uk). Each foot is equipped with a modified Piezo transducer (DN 0714071 from Farnell) to sense ground contact events. We constrain the robot only in the saggital plane by a boom. All three axes (pitch, roll, and yaw) of the boom can rotate freely (see figure 1 C), thus having no influence

on the dynamics of the robot in the sagittal plane. Note that the robot is not supported by the boom in the saggittal plane. In fact, it is always prone to trip and fall.

The most important consideration in the mechanical design of our robot is the location of its center of mass. Its links are made of aluminium alloy, which is light and strong enough. The motor of each hip joint is a HS-475HB from Hitec. It weighs 40g and can output a torque up to 5.5kgcm. Due to the effect of the mechanical stop, the motor of the knee joint bears a smaller torque than the hip joint in stance phases, but must rotate quickly during swing phases for foot clearance. We use a PARK HPXF from Supertec on the knee joint, which is light (19g) but fast with 21rad/s. Thus, about seventy percent of the robot's weight is concentrated on its trunk. The parts of the trunk are assembled in such a way that its center of mass is located as far forward as possible (see figure 2). The effect of this design is illustrated in figure 2. As shown, one walking step includes two stages, the first from (A) to (B), the second from (B) to (C). During the first stage, the robot has to use its own momentum to rise up on the stance leg. When walking at a low speed, the robot may have not enough momentum to do this. So, the distance the center of mass has to cover in this stage should be as short as possible, which can be fulfilled by locating the center of mass of the trunk far forward. In the second stage, the robot just falls forward naturally and catches itself on the next stance leg (see figure 2). Then the walking cycle is repeated. The figure also shows clearly the movement of the curved foot of the stance leg. A stance phase begins with the heel touching ground, and terminates with the toe leaving ground.

3 The neural structure of our reflexive controller

The reflexive controller model of Cruse et al. (1998), and Cruse and Saavedra (1996) that has been applied on many robots can be roughly divided into two levels, the single leg level and the inter-leg level. Figure 3 illustrates how Cruse's model creates a single leg movement pattern. A protracting leg switches to retraction as soon as it attains the AEP (Anterior Extreme Position). A retracting leg switches to protraction when it attains the PEP (Posterior Extreme Position). On the inter-leg level, six different mechanisms

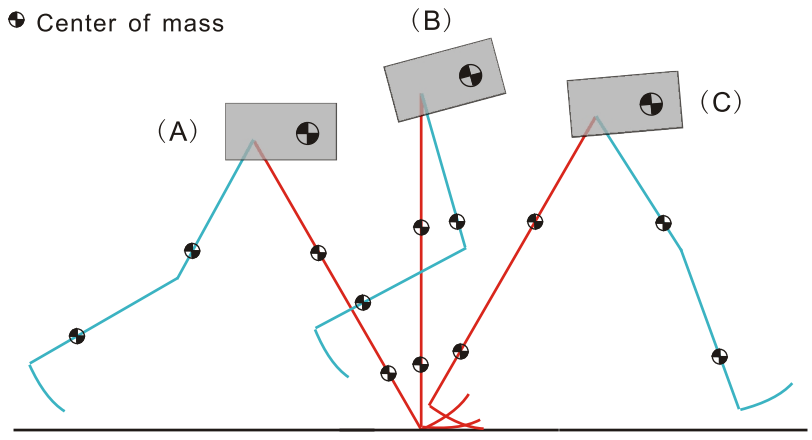

Figure 2: Illustration of a walking step of the robot.

have been described (Cruse et al., 1998), which coordinate leg movements via modifying the AEP and PEP of a receiving leg according to the state of a sending leg.

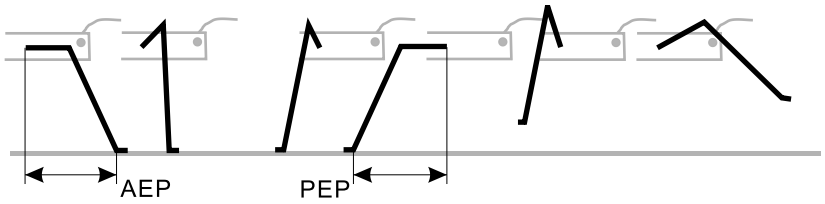

Figure 3: Single leg movement pattern of Cruse's reflexive controller model (Cruse et al., 1998).

Although Cruse's model, as a reflexive controller, is for hexapod locomotion, where the problem of inter-leg coordination is much more complex than in biped walking, we can still compare its mechanism for the generation of single leg movement patterns with that of our reflexive controller. Cruse's model depends on PEP, AEP and GC (Ground Contact) signals to generate the movement pattern of the individual legs. Whereas our reflexive controller presented here uses only GC and AEA (Anterior Extreme Angle of hip joints) to trigger switching between stance and swing phases of each leg. Creation of the single leg movement pattern for our model is illustrated in figure 4.

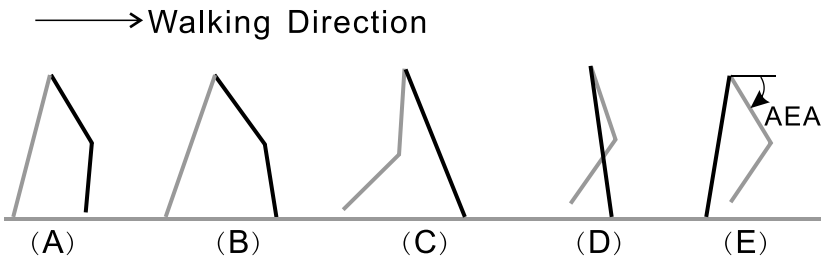

Figure 4: Illustration of single leg movement pattern generation.

Fig. 4 (A)-(E) represents a series of snapshots of the robot configuration while it is walking. At the time of figure 4 B, the left foot (black) has just touched the ground. This event triggers four local joint reflexes at the same time: flexor of left hip, extensor of left knee, extensor of right hip, and flexor of right knee. At the time of figure 4 E, the right hip joint attains its AEA, which triggers only the extensor reflex of the right knee. When the right foot (gray) contacts the ground, a new walking cycle will begin. Note that on the hip joints and knee joints, extensor means forward movement while flexor means backward movement.

The reflexive walking controller of our robot follows a hierarchical structure (see figure 5). The bottom level is the reflex circuit local to the joints, including motor-neurons and angle sensor neurons involved in joint reflexes. The top level is a distributed neural network consisting of hip stretch receptors, ground contact sensor neurons, and inter-neurons for reflexes. Neurons are modelled as non-spiking neurons simulated on a Linux PC, and communicated to the robot via the DA/AD board. Though somewhat simplified, they still retain some of the prominent neuronal characteristics.

3.1 Model neuron circuit of the top level

The joint coordination mechanism in the top level is implemented with the neuron circuit illustrated in figure 5. Each of the ground contact sensor neurons has excitatory connections to the inter-neurons of the ipsi-lateral hip flexor and knee extensor as well as to the contra-lateral hip extensor and knee flexor. The stretch receptor of each hip has excitatory connections to its ipsi-lateral inter-neuron of the knee extensor, and inhibitory connection to its ipsi-lateral inter-neuron of the knee flexor. Detailed models of the inter-

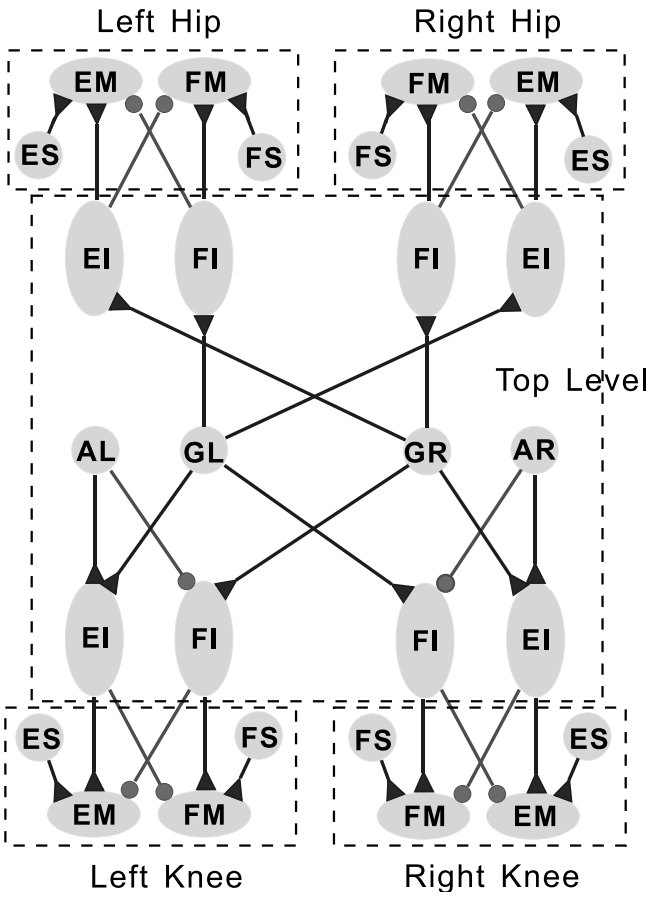

Figure 5: The neuron model of reflexive controller on our robot. Gray circles = Sensor-neurons or Receptors, Vertical ovals = Inter-neurons, horizontal ovals = Motor-neurons. Synapses: black circle = excitatory, black triangle = inhibitory. For meanings of EI, FI, EM, FM, etc. see Table 1.

neuron, stretch receptor, and ground contact sensor neuron are described in following subsections.

3.1.1 Inter-neuron model

The inter-neuron model is adapted from one used in the neural controller of a hexapod simulating insect locomotion (Beer and Chiel, 1992). The state of each model neuron is governed by equations 1,2 (Gallagher et al., 1996):

AL, (AR)	Stretch receptor for anterior angle of left (right) hip
GL, (GR)	Sensor neuron for ground contact of left (right) foot
EI, (FI)	Extensor (Flexor) reflex inter-neuron
EM, (FM)	Extensor (Flexor) reflex motor-neuron
ES, (FS)	Extensor (Flexor) reflex sensor neuron

Table 1: Meaning of some abbreviations used in this paper.

$$\tau_i \frac{dy_i}{dt} = -y_i + \sum \omega_{i,j} u_j \quad (1)$$

$$u_j = (1 + e^{\Theta_j - y_j})^{-1} \quad (2)$$

Where y_i represents the mean membrane potential of the neuron. Equation 2 is a sigmoidal function that can be interpreted as the neuron's short-term average firing frequency, Θ_j is a bias constant that controls the firing threshold. τ_i is a time constant associated with the passive properties of the cell membrane (Gallagher et al., 1996), $\omega_{i,j}$ represents the connection strength from the j th neuron to the i th neuron.

3.1.2 Stretch receptors

Stretch receptors play a crucial role in animal locomotion control. When the limb of an animal reaches an extreme position, its stretch receptor sends a signal to the controller, resetting the phase of the limbs. There is also evidence that phasic feedback from stretch receptors is essential for maintaining the frequency and duration of normal locomotive movements in some insects (Chiel and Beer, 1997).

While other biologically inspired locomotive models and robots use two stretch receptors on each leg to signal the attaining of the leg's AEP and PEP respectively, our robot has only one stretch receptor on each leg to signal the AEA of its hip joint. Furthermore, the function of the stretch receptor on our robot is only to trigger the extensor reflex on the knee joint of the same leg, rather than to explicitly (in the case of CPG models) or implicitly (in the case of reflexive controllers) reset the phase relations between different legs.

As a hip joint approaches the AEA, the output of the stretch receptors for the left (AL) and the right hip (AR) are increased as:

$$\rho_{AL} = (1 + e^{\alpha_{AL}(\Theta_{AL} - \phi)})^{-1} \quad (3)$$

$$\rho_{AL} = (1 + e^{\alpha_{AR}(\Theta_{AR} - \phi)})^{-1} \quad (4)$$

Where ϕ is the real time angular position of the hip joint, Θ_{AL} and Θ_{AR} are the hip anterior extreme angles whose value are tuned by hand in an experiment, α_{AL} and α_{AR} are positive constants. This model is inspired by a sensor neuron model presented in Wadden and Ekeberg (1998) that is thought capable of emulating the response characteristics of populations of sensor neurons in animals.

3.1.3 Ground contact sensor neurons

Another kind of sensor neuron incorporated in the top level is the ground contact sensor neuron, which is active when the foot is in contact with the ground. Its output, similar to that of the stretch receptors, changes according to:

$$\rho_{GL} = (1 + e^{\alpha_{GL}(\Theta_{GL} - V_L + V_R)})^{-1} \quad (5)$$

$$\rho_{GR} = (1 + e^{\alpha_{GR}(\Theta_{GR} - V_R + V_L)})^{-1} \quad (6)$$

Where V_L and V_R are the output voltage signals from piezo sensors of the left foot and right foot respectively, Θ_{GL} and Θ_{GR} work as thresholds, α_{GL} and α_{GR} are positive constants.

While AEP and PEP signals account for switching between stance phase and swing phase in other walking control structures, ground contact signals play a crucial role in phase transition control of our reflexive controller. This emphasized role of the ground contact signal also has some biological plausibility. When held in a standing position on a firm flat surface, a newborn baby will make stepping movements, alternating flexion and extension of each leg, which looks like "walking". This is called "stepping reflex", elicited by the foot's touching of a flat surface. There is considerable evidence that the stepping reflex, though different from actual walking, eventually develops into independent walking (Yang et al., 1998).

Concerning its non-linear dynamics, the biped model is hybrid in nature, containing continuous (in swing phase and stance phase) and discrete (at the ground contact event) elements. Hurmuzlu applied discrete mapping

techniques to study the stability of bipedal locomotion (Hurmuzlu, 1993). It was found that the timing of ground contact events has a crucial effect on the stability of biped walking.

Our preference for using a ground contact signal instead of PEP or AEP signals also has other reasons. In PEP/AEP-models, the movement pattern of a leg will break down as soon as the AEP or PEP can not be reached, which may happen as a consequence of an unexpected disturbance from the environment or due to intrinsic failure. This can be catastrophic for a biped, though tolerable for a hexapod due to its high degree of redundancy.

3.2 Neural circuit of the bottom level

In animals, a reflex is a local motor response to a local sensation. It is triggered in response to a suprathreshold stimulus. The quickest reflex in animals is the "monosynaptic reflex", in which the sensor neuron directly contacts the motor-neuron. The bottom-level reflex system of our robot consists of reflexes local to each joint (see figure 5). The neuron module for one reflex is composed of one angle sensor neuron and the motor-neuron it contacts (see figure 5). Each joint is equipped with two reflexes, extensor reflex and flexor reflex, both are modelled as a monosynaptic reflex, that is, whenever its threshold is exceeded, the angle sensor neuron directly excites the corresponding motor-neuron. This direct connection between angle sensor neuron and motor-neuron is inspired by a reflex described in cockroach locomotion (Beer et al., 1997). In addition, the motor-neurons of the local reflexes also receive an excitatory synapse and an inhibitory synapse from the inter-neurons of the top level, by which the top level can modulate the bottom level reflexes.

Each joint has two angle sensor neurons, one for the extensor reflex, and the other for the flexor reflex (see figure 5). Their models are similar to that of the stretch receptors described above. The extensor angle sensor neuron changes its output according to:

$$\rho_{ES} = (1 + e^{\alpha_{ES}(\phi - \Theta_{ES})})^{-1} \tag{7}$$

where ϕ is the real time angular position obtained from the potentiometer of the joint (see figure 1 B). Θ_{ES} is the threshold of the extensor reflex (see figure 1 B) and α_{ES} a positive constant.

Likewise, the output of the flexor sensor neuron is modelled as:

$$\rho_{FS} = (1 + e^{\alpha_{FS}(\Theta_{FS} - \phi)})^{-1} \tag{8}$$

with Θ_{FS} and α_{FS} similar as above.

It should be particularly noted that the thresholds of the sensor neurons in the reflex modules do not work as desired positions for joint control, because our reflexive controller does not involve any exact position control algorithms that would ensure that the joint positions converge to a desired value. In fact, as will be shown in the next section, the joints often pass these thresholds in swing- and stance phase, and begin their passive movement thereafter.

The sensor-neurons involved in the local reflex module of each joint can only affect the movements of the joint they belong to, having not direct or indirect connection to other joints. This is different for the phasic feedback signal, AEA, which works in the top level (i.e., the inter-joint level), sensing the position of the hip joints and contacting the motor neurons of the knee joints.

The model of the motor-neuron is the same as that of the inter-neurons presented in 3.1.1. Note that, on this robot, the output value of the motor-neurons, after multiplication by a gain coefficient, is sent to the servo amplifier to directly drive the joint motor[1]. In this way, the neural dynamics are directly coupled with the motor dynamics, and furthermore, with the biped walking dynamics. Thus, the robot and its neural controller constitute a closely coupled neuro-mechanical system.

The voltage of joint motor is determined by

$$Motor\ Voltage = M_{AMP}(g_{EM}u_{EM} + g_{FM}u_{FM}), \tag{9}$$

where M_{AMP} represents the magnitude of the servo amplifier, g_{EM} and g_{FM} are output gains of the motor-neurons of the extensor- and flexor reflex respectively, u_{EM} and u_{FM} are the outputs of the motor-neurons.

[1]While we use motors to drive the robot, animals use muscles for walking. Muscles have their own special properties that make them particularly suitable for walking behaviors, for example, the "preflex", which refers to the nonlinear, passive visco-elastic properties of the musculoskeletal system of animals (Brown and Loeb, 1999). Due to the physical nature of the preflex, the system can respond to disturbances rapidly. In the next stage of our work, we will build a Hill-type muscle model with RC motors. The motor-neurons of our reflexive controller at the moment drive the motors directly. In the next stage, they will drive the muscle model directly, just like in animals.

	Θ_{EI}	Θ_{FI}	Θ_{EM}	Θ_{FM}	α_{ES}	α_{FS}
Hip Joints	5	5	5	5	4	1
Knee Joints	5	5	5	5	4	4

Table 2: Parameters of neurons for hip- and knee joints. For meaning of the subscripts, see table 1.

Θ_{GL} (v)	Θ_{GR} (v)	Θ_{AL} (deg)	Θ_{AR} (deg)	α_{GL}	α_{GR}	α_{AL}	α_{AR}
2	2	$= \Theta_{ES}$	$= \Theta_{ES}$	4	4	4	4

Table 3: Parameters of stretch receptors and ground contact sensor neurons.

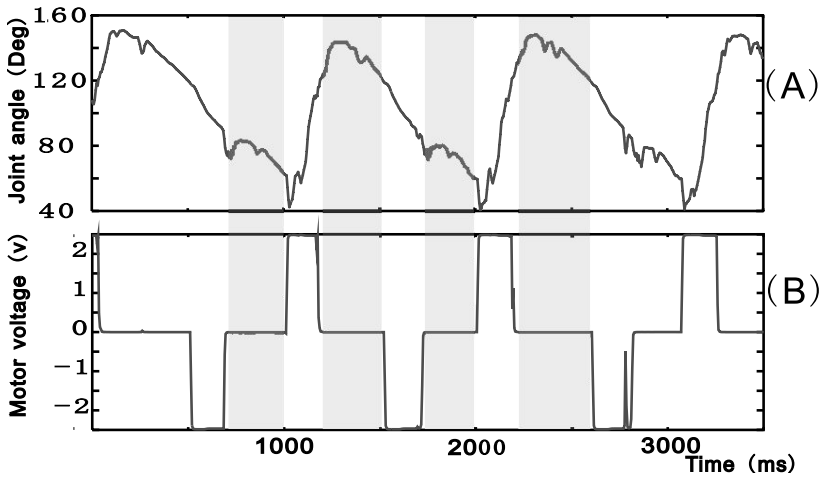

Figure 6: Realtime data of one hip joint. (A) Hip joint angle. (B) Motor voltage measured directly at the motor-neurons of the hip joint. During some periods (the gray areas), the motor voltage remains zero, and the hip joint moves passively.

4 Robot walking experiments

The model neuron parameters chosen jointly for all experiments are listed in Table 2 and 3. Only the thresholds of the sensor neurons and the output gain of the motor-neurons are changed in different experiments. The time constants τ_i of all neurons take the same value of 5ms. The weights of all the inhibitory connections are set to -10. The weights of all excitatory connec-

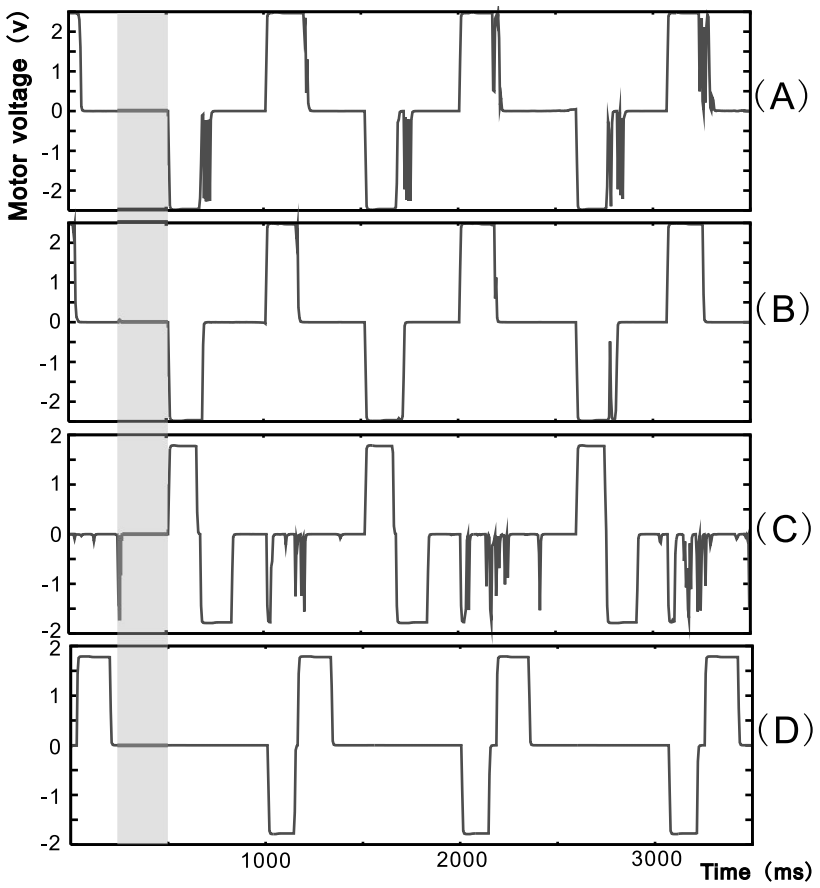

Figure 7: Motor voltages of the four joints measured directly at the motor-neurons, while the robot is walking: (A) left hip; (B) right hip; (C) left knee; (D) right knee. Note that during one period of every gait cycle (gray area), all four motor voltages remain zero, and all four joints (i.e., the whole robot) move passively (see figure 8).

tions are 10, except those between inter-neurons and motor-neurons, which are 0.1.

We encourage readers to watch the video clips of the robot walking experiments:
Walking fast on a flat floor, http://www.cn.stir.ac.uk/~tgeng/robot/walkingfast.mpg
Walking with a medium speed, http://www.cn.stir.ac.uk/~tgeng/robot/walkingmedium.mpg

	Θ_{ES} (deg)	Θ_{FS} (deg)	g_{EM}	g_{FM}
Hip Joints	115	70	± 2	± 2
Knee Joints	180	100	± 1.8	± 1.8

Table 4: Specific parameters for walking experiments.

Walking slowly http://www.cn.stir.ac.uk/~tgeng/robot/walkingslow.mpg
Climbing a shallow slope, http://www.cn.stir.ac.uk/~tgeng/robot/climbingslope.mpg

These videos can be viewed with Windows Media Player (www.microsoft.com) or Realplayer (www.real.com).

4.1 Passive movements of the robot

In a walking experiment with specific parameters as given in table 6 the passive part of the movement of the robot is shown most clearly. (The sign of g_{EM} and g_{FM} depends on the hardware configurations of the motors on the left and right leg).

Figure 6 shows the motor voltage and the angular movement of one of its hip joints while the robot is walking. During roughly more than half of every gait cycle, the hip joint is moving passively.

As shown in figure 7, during some period of every gait cycle (e.g., grey area in figure 7), the motor voltages of the motor-neurons on all four joints remain zero, so all joints move passively until the swing leg touches the ground (see figure 8). During this time, which is roughly one third of a gait cycle (see figure 7 and figure 8), the movement of the whole robot is exclusively under the control of "physical computation" following its passive dynamics; no feedback based active control acts on it. This demonstrates very clearly how neurons and mechanical properties work together to generate the whole gait trajectory. This is also analogous to what happens in animal locomotion. Muscle control of animals usually exploits the natural dynamics of their limbs. For instance, during the swing phase of the human walking gait, the leg muscles first experience a power spike to begin leg swing and then remain limp throughout the rest of the swing phase, similar to what is shown in figure 8. Note that, in figure 8 and the corresponding stick diagrams of walking gait, we omitted the detailed movement of the curved foot, in order to show clearly the leg-movements. The point on which the

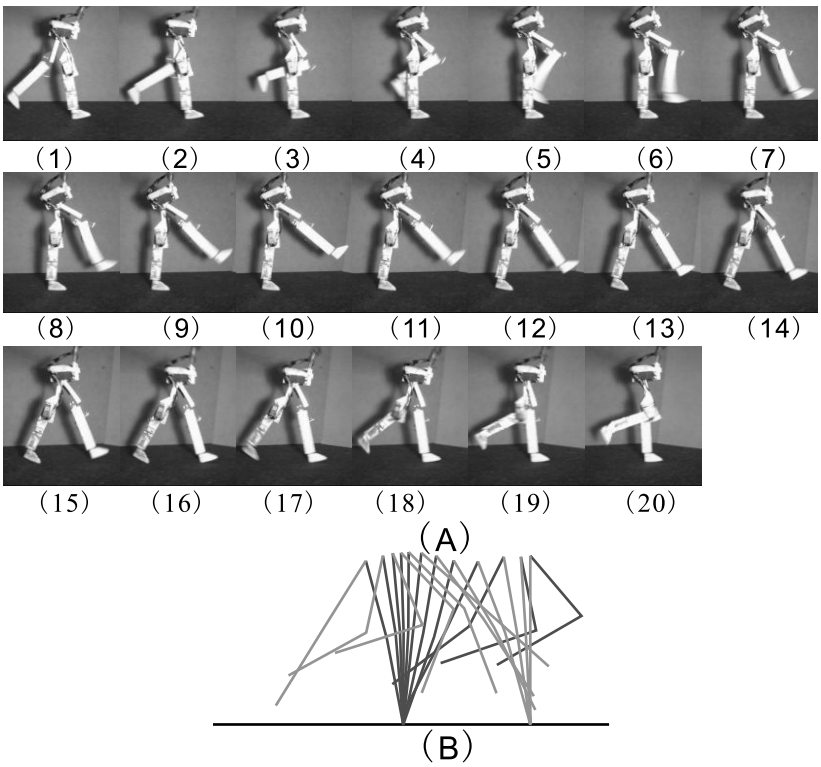

Figure 8: A). A series of sequential frames of a walking gait cycle. The interval between every two adjacent frames is 33 ms. Note that, during the time between frame (10) and frame (15), which is nearly one third of the time length of a gait cycle (corresponding to the grey area in figure 7), the robot is moving passively. At the time of frame (15), the swing leg touches the floor and a new gait cycle begins. (B). Stick diagram of the gait drawn from the frames in (A). The interval between any two consecutive snapshots is 67 ms.

stance leg stands is the orthographic projection of the mid-point of the foot and not its exact ground-contact point.

4.2 Walking at different speeds and a perturbed gait

The walking speed of the robot can be changed easily by adjusting only the thresholds of the reflex sensor neurons and the output gain of the motor-neurons (see table 5). Figure 9 A and B show two phase plots of the hip and

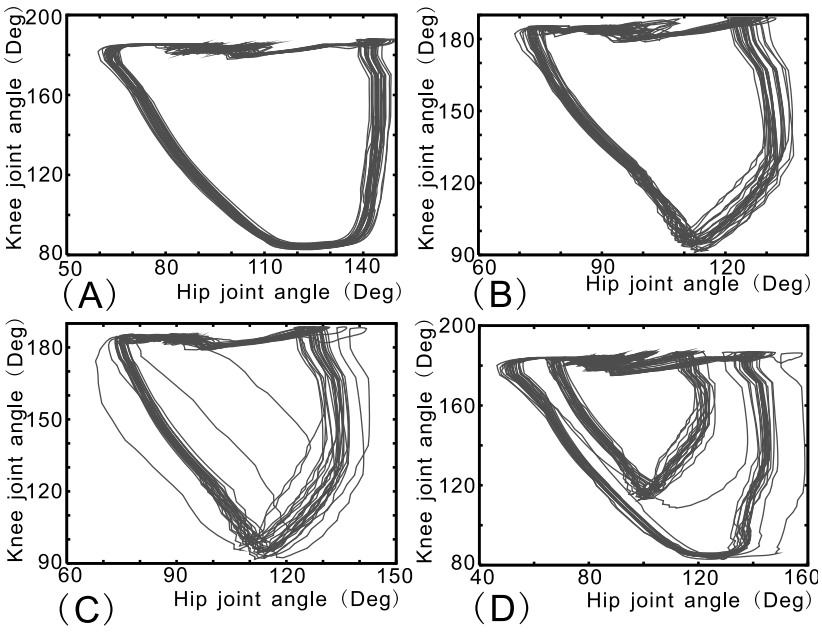

Figure 9: Phase diagrams of hip joint position and knee joint position of one leg. Robot speed: (A) 28cm/s; (B) 63cm/s. (C) A perturbed walking gait. For values of the neuron parameters chosen in these experiments, see table 6. Note that the hip joint angle in these figures is an absolute value, not the angle relative to the robot body as shown in Fig. 1 B. (D) The walking speed is changed online.

knee joint positions, which were recorded while the robot was walking with different speeds on a flat floor.

Figure 9 C shows a perturbed walking gait. The bulk of the trajectory represents the normal orbit of the walking gait, while the few outlaying trajectories are caused by external disturbances induced by small obstacles such as thin books (less than four percent of robot size) obstructing the robot path. After a disturbance, the trajectory returns to its normal orbit soon, demonstrating that the walking gaits are stable and to some degree robust against external disturbances. Here robustness is defined as rapid convergence to a steady state behavior despite unexpected perturbations (Lewis, 2001).

With neuron parameters changed in the cases of fast walking and slow

		Θ_{ES} (deg)	Θ_{FS} (deg)	g_{EM}	g_{FM}
Low speed walking	Hip Joints	120	70	± 1.4	± 1.3
see Fig. 9 A	Knee Joints	180	100	± 1.5	± 1.5
High speed walking	Hip Joints	110	85	± 2.5	± 2.5
see Fig. 9 B	Knee Joints	180	100	± 1.8	± 1.8
Perturbed walking gait	Hip Joints	115	90	± 2.5	± 2.5
see Fig. 9 C	Knee Joints	180	100	± 1.5	± 1.5

Table 5: The different values of neuron parameters chosen to generate different speeds (see figure 9).

walking, walking dynamics are implicitly drawn into a different gait cycle (see figure 9). Figure 9 D shows an experiment in which the neuron parameters are changed abruptly online while the robot is walking at a slow speed (33cm/s, the big orbit). After a short transient stage (the outlaying trajectories), the gait cycle of the robot is automatically transferred into another stable, high-speed orbit (the small one, 57cm/s). In other words, when the neuron parameters are changed, physical computation closely coupled with neural computation can autonomously shift the system into another global trajectory that is also dynamically stable. This experiment shows that our biped robot, as a neuro-mechanical system, is stable in a relatively large domain of its neuron parameters.

With other real-time biped walking controllers based on biologically inspired mechanisms (e.g., CPG) or conventional trajectory preplanning and tracking control, it is still a puzzling problem how to change walking speed on the fly without undermining dynamical stability at the same time. However, this experiment shows that the walking speed of our robot can be drastically changed (nearly doubled) on the fly while the stability is still retained due to physical computation.

4.3 Walking up a shallow slope

Figure 10 is a stick diagram of the robot when it is walking up a shallow slope of about 4 degrees. Steeper slopes could not be mastered. In figure 10, we can see that, when the robot is climbing the slope, its step length is becoming smaller, and the movement of its stance leg is becoming slower (its stick

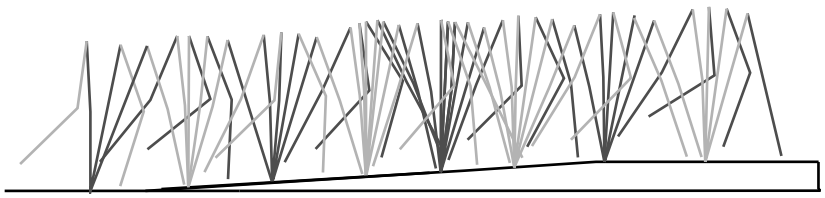

Figure 10: The robot is climbing a shallow slope. The interval between any two consecutive snapshots is 67 ms.

snapshots are becoming denser). Note that these adjustments of its gait take place autonomously due to the robot's physical properties (physical computation), not relying on any pre-planned trajectory or precise control mechanism. This experiment demonstrates that such a closely coupled neuro-mechanical system can to some degree autonomously adapt to an unstructured terrain.

5 Stability analysis of the walking gaits

5.1 Dynamic model of the robot

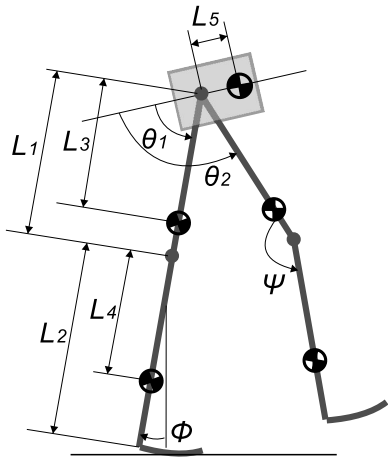

Figure 11: Model of the dynamics of our robot. Sizes and masses are the same as those of the real robot.

The dynamics of our robot are modelled as shown in figure 11. With the

Lagrange method, we can get the equations that govern the motion of the robot, which can be written in the form:

$$D(q)\ddot{q} + C(q, \ddot{q}) + G(q) = \tau \tag{10}$$

Where $q = [\phi, \theta_1, \theta_2, \psi]^T$ is a vector describing the configuration of the robot (for definition of $\phi, \theta_1, \theta_2, \psi$, see figure 11). $D(q)$ is the 4×4 inertia matrix, $C(q, \ddot{q})$ is the 4×1 vector of centripetal and coriolis forces, $G(q)$ is the 4×1 vector representing gravity forces. $\tau = [0, \tau_1, \tau_2, \tau_3]^T$, τ_1, τ_2, τ_3 are the torques applied on the stance hip (the hip joint of the stance leg in figure 11), the swing hip, and the swing knee joints, respectively. Details of this equation can be found in the appendix.

The dynamics of the DC motor (including gears) of each joint can be described with the following equations (here, the hip of the stance leg is taken as an example. The models of other joints are likewise):

$$L_a \frac{di_a}{dt} + R_a i_a + n k_3 \dot{\theta_1} = V_1 \tag{11}$$

$$\tau_1 + I_1 \ddot{\theta_1} + k_f \dot{\theta_1} = n k_2 i_a \tag{12}$$

Where, V_1 is the applied armature voltage of the stance hip motor, which is obtained from the output of the motor neurons according to equation 9, i_a is the armature current, L_a the armature inductance, R_a the armature resistance. k_3 is the emf constant. k_2 is the motor torque constant. I_1 is the combined moment of inertial of the stance-hip motor and gear train referred to the gear output shaft. k_f is the vicious-friction coefficient of the combination of the motor and the gear. n is the gear ratio.

Considering that the electrical time-constant of the motor is much smaller than the mechanical time-constant of the robot, we neglect the dynamics of the electrical circuits of the motor, which leads to, $\frac{di_a}{dt} = 0$. Thus equation 11 is reduced to,

$$i_a = \frac{1}{R_a}(V_1 - n k_3 \dot{\theta_1}) \tag{13}$$

Combining equations 10, 12 and 13, we can get the dynamics model of the robot with the applied motor voltages as its control input.

The heel strike at the end of swing phases and the knee strike at the end of knee extensor reflex are assumed to be inelastic impacts, which is in

accordance with observations on our real robot and existing passive biped robots. This assumption implies the conservation of angular momentum of the robot just before and after the strikes, with which the value of $\dot{q}$ just after the strikes can be computed using its value just before the strikes. Because the transient double support phase is very short in our robot walking (usually less than 40 ms), it is neglected in our simulation as often done in the analysis of other passive bipeds (Garcia, 1999).

5.2 Stability analysis with Poincare maps

The method of Poincare maps is usually employed for stability analysis of cyclic movements of non-linear dynamic systems such as passive bipeds (Garcia, 1999). Because our reflexive controller exploits natural dynamics for the robot's motion generation, and not trajectory planning or tracking control, the Poincare map approach can also be applied to the dynamics model of our robot together with the reflexive network as its controller.

We choose the Poincare section (Garcia, 1999) to be right after the heel strike of the swing leg. Each cyclic walking gait is a limit cycle in the state space, corresponding to a fixed point on the Poincare section. Fixed points can be found by solving the roots of the mapping equation:

$$P(x^n) - x^n = 0 \tag{14}$$

Where $x^n = [q, \dot{q}]^T = [\phi, \theta_1, \theta_2, \psi, \dot{\phi}, \dot{\theta_1}, \dot{\theta_2}, \dot{\psi}]^T$ is a state vector on the Poincare section at the beginning of the n_{th} gait cycle. $P(x^n)$ is a map function mapping x^n to x^{n+1}, which is built by combining the reflexive controller and the robot dynamics model described above.

Near a fixed point, x^*, the map function $P(x^*)$ can be linearized as (Garcia, 1999):

$$P(x^* + \hat{x}) \approx P(x^*) + J\hat{x} \tag{15}$$

Where J is the 8×8 Jacobian matrix of partial derivatives of P

$$J = \frac{\partial P}{\partial x} \tag{16}$$

With any fixed point, J can be obtained by numerically evaluating P eight times in a small neighborhood of the fixed point. According to equation 15, small perturbations $\hat{x}^i$ to the limit cycle x^* at the start of ith step will grow

Table 6: Fixed parameters of the knee joints.

	$\Theta_{ES,k}$ (deg)	$\Theta_{FS,k}$ (deg)	$G_{M,k}$
Knee Joints	180	110	$0.9G_{M,h}$

or decay from the ith step to the $i+1$th step approximately according to $\hat{x}^{i+1} \approx J\hat{x}^i$. So, if all eigenvalues of J lie within the unit cycle, any small perturbation will decay to 0 and the perturbed walking gait will return to its limit cycle, which means the limit cycle is asymptotically stable (Garcia, 1999).

The movements of the knee joints are needed mainly for timely ground clearance without much influence on the stability of the walking gait. Therefore, in the simulation analysis and real experiment below we set the knees' neuron parameters to fixed values (see Table 6) that can ensure fast movements of the knee joints, preventing any possible scuff of the swing leg.

For simplicity, we also fix the threshold of the flexor sensor neurons of the hips ($\Theta_{FS,h}$) to 85 deg in simulation and real experiments below. This will not damage the generality of the results, because similar results can be obtained provided that $\Theta_{FS,h}$ is in the interval 70-90 deg. For values outside this range the robot will either fall or produce gaits which are very unnatural. Thus, now we only need to tune two parameters of the hip joints: the threshold of the extensor sensor neurons ($\Theta_{ES,h}$) and the gain of the motor-neurons of hip joints ($G_{M,h}$), which work together to determine the gait properties. $\Theta_{ES,h} - \Theta_{FS,h}$ determines roughly the stride length (not exactly, because the hip joint moves passively after passing $\Theta_{ES,h}$), while $G_{M,h}$ determines the amplitude of the applied voltage of the motors on the hip joint. Since these two parameters have such clear physical interpretations, their tuning is straightforward.

With each set of the controller parameter $\Theta_{ES,h}$ and $G_{M,h}$, we use a multi-dimensional Newton-Raphson method solving equation 14 to find the fixed point (Garcia, 1999). Then we compute the Jacobian matrix J of the fixed point using the approach described above, and evaluate the stability of the fixed point according to its eigenvalues. The result of this Poincare map analysis is shown in figure 12. We have found that asymptotically stable fixed points exist in a considerably large range of the controller parameters $\Theta_{ES,h}$ and $G_{M,h}$ (see figure 12). For comparison, figure 12 also shows the

stable range of these two parameters obtained in real robot experiments. In the real robot, because no definite stability criterion, like using eigenvalues, is applicable, we regard a walking gait as stable if the robot does not fall.

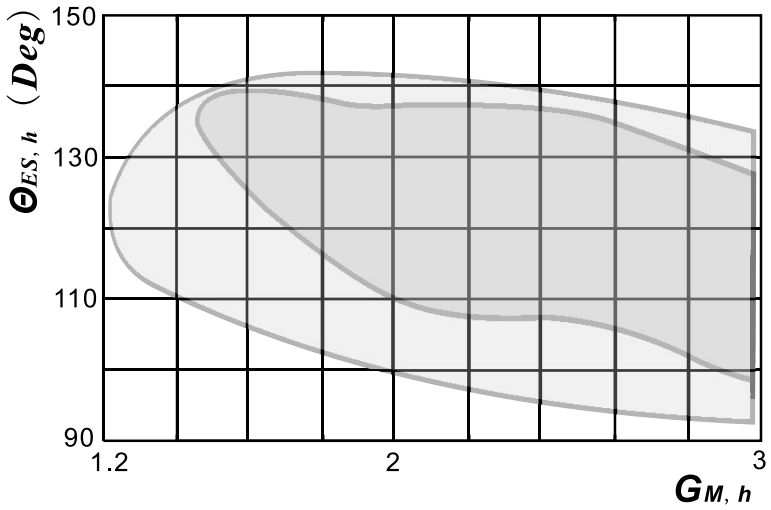

Figure 12: Stable domain of the controller parameter, $\Theta_{ES,h}$ and $G_{M,h}$. The big area enclosed by the outer curve represents the range obtained with simulations in which fixed points are stable. The shaded area is the range of the two parameters, in which stable gaits will appear in experiments performed with the real robot. The maximum permitted value of $G_{M,h}$ is 2.95 (higher values will destroy the motor of the hip joint). The two closed curves are a manual, continuous interpolation of the discrete boundaries obtained in simulations and real experiments, respectively.

The best way to visualize the properties of a limit cycle is using the phase plane, which can be easily obtained in the simulations, but is not available in our real robot due to the lack of absolute position- and speed sensors. Figure 13 shows two phase plane plots of the absolute angular position of one hip joint, ϕ (see figure 11) and its derivative, $\dot{\phi}$. After being perturbed, the walking gait returns to its limit cycle quickly in only a few steps, which is in accordance with the experiment results of the real robot presented in the last section.

Because some details of the robot dynamics such as uncertainties of the ground contact, nonlinear frictions in the joints and the inevitable noise and lag of the sensors are difficult, if not impossible, to model precisely, the results of simulation and real experiments are not exactly coherent (see

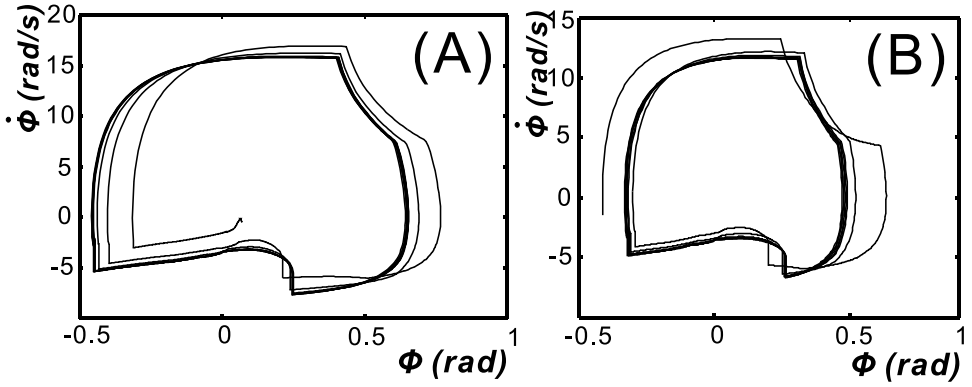

Figure 13: Two limit cycles in the phase plan of ϕ and $\dot{\phi}$. (A) is corresponding to a fixed point found with this set of controller parameters, $\Theta_{ES,h} = 125Deg$, $G_{M,h} = 2.8$, (B) corresponding to $\Theta_{ES,h} = 110Deg$, $G_{M,h} = 2.5$

figure 12). However, stability analysis and experiments with our real robot have in general shown that our biped robot under control of the reflexive network will demonstrate stable walking gaits in a wide range of the critical controller parameters and that it will return to its normal orbit quickly after a disturbance.

6 Discussion and comparison with other walking control mechanisms

6.1 Minimal set of phasic feedbacks

The aim of locomotion control structures (modelled either with CPG or with reflexive controllers) is to control the phase relations between limbs or joints, attaining a stable phase locking that leads to a stable gait. Therefore, the locomotion controller needs phasic feedback from the legs or joints. In the case of reflexive controllers like Cruse's model (Cruse et al., 1998), the phasic feedback signals sent to the controller are AEP and PEP signals, which can provide sufficient information on phase relations at least between adjacent legs. It is according to this information that the reflexive controller adjusts the PEP value of the leg, thus effectively changing the period of the leg, synchronizing it in, or out of phase with its adjacent legs (Klavins et al.,

2002). On the other hand, in the case of a CPG model, which can generate rhythmic movement patterns even without sensory feedback, it must nonetheless be entrained to phasic feedback from the legs in order to achieve realistic locomotion gaits. In some animals, evidence exists that every limb involved in cyclic locomotion has its own CPG (Delcomyn, 1980), and phasic feedback from muscles is indispensable to keep its CPGs in phase with the real time movement of the limbs. Not surprisingly, CPG mechanisms used on various locomotive robots also require phasic feedback. Lewis et al. (2003) implemented a CPG oscillator circuit to control a simple biped. AEP and PEP signals from its hip joints define the feedback to the CPG, resetting its oscillator circuit. Removal of the AEP or PEP signals caused quick deterioration of this biped's gait. On another quadruped robot (Fukuoka et al., 2003), instead of discrete AEP and PEP signals, continuous position signals of the hip joints provide feedback to the neural oscillators of the CPG. The neural oscillator parameters were tuned in such a way that the minimum and maximum of the hip positions would reset the flexor- and extensor oscillator respectively. Apparently, this scheme functions identically with AEP, PEP feedback.

In summary, because AEP and PEP provide sufficient information about phase relations between legs, walking control structures usually depend on them (or their equivalents) as phasic feedback from the legs. However, the top level of the reflexive controller on our robot requires only AEA signals as phasic feedback. Furthermore, this AEA signal is only for triggering the flexor reflex on the knee joint of the robot, rather than triggering stance phases as in other robots. In this sense, the role (and number) of the phasic feedback signals is much reduced in our reflexive controller.

In spite of the fact that the AEA signal is by itself not sufficient to control the phase relations between legs, stable walking gaits have appeared in our robot walking experiments (see section 4). This is because reflexive controller and physical computation cooperate to accomplish the task of phasic walking gait control. This shows that physical computation can help to simplify the controller structure.

As described above, CPGs have been successfully applied on some real-time quadruped, hexapod and other multi-legged robots. However, in biped walking control based on CPG models, most of the current studies are performed with computer simulations. To our knowledge, no one has successfully realized real-time dynamic biped walking using a CPG model as a single controller, because the CPG model itself can not ensure stability of the biped

gait. A considerably well-known biped robot controlled by a CPG chip has been developed by Lewis et al. (2003). Its walking/running gaits looks very nice, though on a treadmill instead of on a floor. But this biped robot has a fatally weak point in that its hips are fixed on a boom (not rotating freely around the boom axes as in our robot). So it is actually supported by the boom. The boom is greatly facilitating its control, avoiding the most difficult problem of dynamic stability control that is specific to biped robots. Thus, this robot is indeed not a dynamic biped in its real sense. Instead, it is rather more equivalent to one pair of legs of a multi-legged robot.

Using computer simulations, Taga (1995) found that stable biped gaits can be generated by combining CPGs and human biomechanics. In animals, a CPG is a neural structure which is much more complex than the local reflex in anatomy and function. There is evidence that, in mammal- and human locomotion, CPGs work on top of reflexes and take their effects via modulating them. In evolution, simple monosynaptic reflexes must have appeared much earlier than the much more complex CPG structures. Not only with simulation analysis, but also with our real system experiments, the current study has shown that local neuronal reflexes connected by a simple sensor-driven network are sufficient as a controller for dynamic biped walking, the most difficult form of legged locomotion in view of dynamic stability.

6.2 Physical computation and approximation

In contrast to exact representations and world models, physical computation often implies approximation. Approximation in control mechanism gives more room and possibility for physical computation. While conventional robots rely on precise trajectory planning and tracking control, biologically inspired robots rarely use preplanned or explicitly computed trajectories. Instead, they compute their movements approximately by exploiting physical properties of their self and the world, thus avoiding the accurate calibration and modelling required by conventional robotics. But, in order to achieve real time walking gait in a real world, even these biological inspired robots often have to depend on some kinds of position- or velocity control on their joints. For example, on a hexapod, simulating the distributed locomotion control of insects (Beer et al., 1997), outputs of motor-neurons were integrated to produce a trajectory of joint positions that was tracked using proportional feedback position control. On a quadruped, built by Kimura's group, that implemented CPGs (neural oscillators) and local reflexes, all joints are PD

controlled to move to their desired angles (Fukuoka et al., 2003). Even on a half passive biped, controlled by a CPG chip, position control worked on its hip joints, though passive dynamics of its knee joints was exploited for physical computation (Lewis, 2001).

The principle of approximation embodied in the reflexive controller of our robot, however, goes even one step further, in the sense that there is no position or velocity control implemented on our robot. The neural structure of our reflexive controller does not depend on, or ensure the tracking of, any desired position. Indeed, it is this approximate nature of our reflexive controller that allows the physical properties of the robot itself, especially the passive dynamics of the robot (see figure 8), to contribute implicitly to generation of overall gait trajectories, and ensures its stability and robustness to some extent. Just as argued by Raibert and Hodgins 1993, page 353, "Many researchers in neural motor control think of the nervous system as a source of commands that are issued to the body as direct orders. We believe that the mechanical system has a mind of its own, governed by the physical structure and the laws of physics. Rather than issuing commands, the nervous system can only make suggestions which are reconciled with the physics of the system and the task."

7 Conclusions

In this paper, we presented our design and some walking experiments performed by a novel neuro-mechanical structure for reflexive walking control. We demonstrated with a closely coupled neuro-mechanical system, how physical computation can be exploited to generate a dynamically stable biped walking gait. In the experiments of walking at different speeds and climbing a shallow slope, it was also shown that the coupled dynamics of this neuro-mechanical system are sufficient to induce an autonomous, albeit limited, adaptation of the gait.

While the biologically inspired model neurons used in our reflexive controller retain some properties of real neurons, they do not include one of the most significant features of neurons, namely synaptic plasticity. As has been observed in human and animal locomotion, while walking gait generation may be reflexive, stability control of walking behavior has to be predictive. Although physical computation can assure autonomy and stability to some extent, in order to get a stable walking gait in a wide parameter range, we

have to rely on the plasticity of the neural structure. In the near future, we will apply proactive learning on this neuro-mechanical system (Porr and Wörgötter, 2003). The basic idea is to use the waveform resulting from the ground contact sensors to predict and thus avoid possible instabilities of the next walking step.

Acknowledgement

This work was supported by SHEFC grant INCITE to Prof. F. Wörgötter. We thank Kevin Swingler for correction of the text.

References

Beer, R. and Chiel, H. (1992). A distributed neural network for hexapod robot locomotion. *Neural Computation*, 4:356–365.

Beer, R., Quinn, R., Chiel, H., and Ritzmann, R. (1997). Biologically inspired approaches to robotics. *Communications of the ACM*, 40(3):30–38.

Boone, G. and Hodgins, J. (1997). Slipping and tripping reflexes for bipedal robots. *Autonomous Robots*, 4(3):259–271.

Brown, I. and Loeb, G. (1999). *Biomechanics and Neural Control of Movement*, chapter A reductionist approach to creating and using neuromusculoskeletal models. Springer-Verlag, New York.

Cham, J., Bailey, S., and Cutkosky, M. (2000). Robust dynamic locomotion through feedforward-preflex interaction. In *ASME IMECE Proceedings*, Orlando, Florida.

Chiel, H. and Beer, R. (1997). The brain has a body: adaptive behavior emerges from interactions of nervous system, body, and environment. *Trends in Neuroscience*, 20:553–557.

Cruse, H., Kindermann, T., Schumm, M., and et.al. (1998). Walknet - a biologically inspired network to control six-legged walking. *Neural Networks*, 11(7-8):1435–1447.

Cruse, H. and Saavedra, M. (1996). Curve walking in crayfish. *Journal of Experimental Biology*, 199:1477–1482.

Cruse, H. and Warnecke, H. (1992). Coordination of the legs of a slow-walking cat. *Experimental Brain Research*, 89:147–156.

Delcomyn, F. (1980). Neural basis of rhythmic behavior in animals. *Science*, 210:492–498.

Ferrell, C. (1995). A comparison of three insect-inspired locomotion controllers. *Robotics and Autonomous Systems*, 16:135–159.

Fukuoka, Y., Kimura, H., and Cohen, A. (2003). Adaptive dynamic walking of a quadruped robot on irregular terrain based on biological concepts. *Int. J. of Robotics Research*, 22:187–202.

Full, R. J. and Tu, M. S. (1990). Mechanics of six-legged runners. *Journal of Experimental Biology*, 148:129–146.

Funabashi, H., Takeda, Y., S., I., and Higuchi, M. (2001). Disturbance compensating control of a biped walking machine based on reflex motions. *JSME International Journal Series C-Mechanical Systems,Machine Elements and Manufacturing*, 44:724–730.

Gallagher, J., Beer, R., Espenschied, K., and Quinn, R. (1996). Application of evolved locomotion controllers to a hexapod robot. *Robotics and Autonomous Systems*, 19:95–103.

Garcia, M. (1999). *Stability, scaling, and chaos in passive-dynamic gait models*. PhD thesis, Cornell University.

Hurmuzlu, Y. (1993). Dynamics of bipedal gait; part ii: Stability analysis of a planar five-link biped. *ASME Journal of Applied Mechanics*, 60(2):337–343.

Iida, F. and Pfeifer, R. (2004). Self-stabilization and behavioral diversity of embodied adaptive locomotion. *Lecture notes in artificial intelligence*, 3139:119–129.

Klavins, E., Komsuoglu, H., Full, R., and Koditschek, D. (2002). *Neurotechnology for Biomimetic Robots*, chapter The Role of Reflexes Versus Central Pattern Generators in Dynamical Legged Locomotion. MIT Press.

Lewis, M. (2001). Certain principles of biomorphic robots. *Autonomous Robots*, 11:221–226.

Lewis, M., Etienne-Cummings, R., Hartmann, M., Xu, Z., and Cohen, A. (2003). An in silico central pattern generator: Silicon oscillator, coupling, entrainment, and physical computation. *Biological Cybernetics*, 88:137–151.

Porr, B. and Wörgötter, F. (2003). Isotropic sequence order learning. *Neural Comp.*, 15:831–864.

Porr, B. and Wörgötter, F. (2005). Inside embodiment what means embodiment for radical constructivists? *Kybernetes*, 34:105–117.

Pratt, J. (2000). *Exploiting Inherent Robustness and Natural Dynamics in the Control of Bipedal Walking Robots*. PhD thesis, Massachusetts Institute of Technology.

Raibert, H. and Hodgins, J. (1993). *Biological Neural Networks in Invertebrate Neuroethology and Robotics*, chapter Legged robots, pages 319–354. Academic Press, Boston.

Reeve, R. (1999). *Generating walking behaviors in legged robots*. PhD thesis, University of Edinburgh.

Taga, G. (1995). A model of the neuro-musculo-skeletal systems for human locomotion. *Biological Cybernetics*, 73:97–111.

Van der Linde, R. Q. V. (1998). Active leg compliance for passive walking. In *Proceedings of IEEE International Conference on Robotics and Automation*, Orlando, Florida.

Wadden, T. and Ekeberg, O. (1998). A neuro-mechanical model of legged locomotion: Single leg control. *Biological Cybernetics*, 79:161–173.

Yang, J., Stephens, M., and Vishram, R. (1998). Infant stepping: A method to study the sensory control of human walking. *J. Physiol (London)*, 507:927–937.

Ziemke, T. (2001). Are robots embodied? In *First international workshop on epigenetic robotics Modeling Cognitive Development in Robotic Systems*.

Appendix

In the following we list the terms of the equation used in the simulation to build the Poincare map function. For definitions of $l_1, l_2, l_3, l_4, l_5, \phi, \theta_1, \theta_2, \psi$, see figure 11. r is the radius of the curved foot. m_t is the mass of the trunk, m_h the mass of the thigh, m_k the mass of the shank with foot. g is the gravity.

$$
\begin{aligned}
D_{11} &= -4m_k \cos(\phi)\, r^2 - 2l_4 l_2 + 2m_k r l_4 + 2m_k {l_1}^2 + {l_2}^2 \\
&+2\ \mathrm{m}_t l_1 l_2 - 2l_1 r - 2m_t r l_2 \\
&+4\ \mathrm{m}_k r \cos(\phi)\, l_2 - 2m_k r \cos(\phi)\, l_4 + 2m_k {l_4}^2 + 2m_t r \cos(\phi)\, l_2 \\
&+2\ \mathrm{m}_t l_2 l_5 \cos(\theta_1) - 2m_t r l_5 \cos(\theta_1) \\
&+2\ \mathrm{m}_t r \cos(\phi)\, l_1 + 2m_t r l_5 \cos(\theta_1 - \phi) + 2m_t l_1 l_5 \cos(\theta_1) \\
&\text{-}2\ \mathrm{m}_t \cos(\phi)\, r^2 + m_t {l_5}^2 \\
&\text{-}4\ \mathrm{m}_h \cos(\phi)\, r^2 - 2m_h l_1 l_3 - 2m_h l_2 l_3 \\
&+2\ \mathrm{m}_h r l_3 + 2m_k l_1 l_2 - 2m_k l_1 r - 4m_k r l_2 + 4m_k r^2 \\
&+2\ \mathrm{m}_k {l_2}^2 + 4m_h l_1 l_2 - 4m_h l_1 r - 4m_h r l_2 \\
&+2\ \mathrm{m}_h {l_1}^2 + 4m_h r^2 + 2m_h {l_2}^2 \\
&\text{-}2\ \mathrm{m}_h r l_3 \cos(-\theta_2 + \phi) \\
&\text{-}2\ \mathrm{m}_h l_1 l_3 \cos(-\theta_1 + \theta_2) - 2m_h l_2 l_3 \cos(-\theta_1 + \theta_2) \\
&+2\ \mathrm{m}_h r l_3 \cos(-\theta_1 + \theta_2) - 2m_k r l_4 \cos(-\theta_2 + \psi) \\
&+2\ \mathrm{m}_k r l_4 \cos(-\theta_1 + \theta_2 + \psi + \phi) \\
&\text{-}2\ \mathrm{m}_k r l_1 \cos(-\theta_1 + \theta_2 + \phi) \\
&\text{-}2\ \mathrm{m}_k l_1 l_4 \cos(\psi) + 2m_k l_4 l_2 \cos(-\theta_1 + \theta_2 + \psi) \\
&+2\ \mathrm{m}_k l_1 l_4 \cos(-\theta_1 + \theta_2 + \psi) \\
&+2\ \mathrm{m}_k r l_1 \cos(-\theta_1 + \theta_2) + 4m_h r \cos(\phi)\, l_2 \\
&\text{-}2\ \mathrm{m}_h r \cos(\phi)\, l_3 + 4m_h r \cos(\phi)\, l_1 \\
&\text{-}2\ \mathrm{m}_k {l_1}^2 \cos(-\theta_1 + \theta_2) \\
&+2\ \mathrm{m}_h {l_3}^2 + m_t {l_1}^2 + 2m_t r^2
\end{aligned}
$$

$$
\begin{aligned}
\mathrm{D}_{12} &= -m_t r l_5 \cos(\theta_1 - \phi) + m_t r l_5 \cos(\theta_1) \\
&\text{-}\mathrm{m}_t (l_1 + l_2) l_5 \cos(\theta_1) \\
&\text{-}\mathrm{m}_t m_h r l_3 \cos(-\theta_1 + \theta_2 + \phi) \\
&\text{-}\mathrm{m}_h r l_3 \cos(-\theta_1 + \theta_2) + m_h l_2 l_3 \cos(-\theta_1 + \theta_2) \\
&+\mathrm{m}_h l_1 l_3 \cos(-\theta_1 + \theta_2) - m_h {l_3}^2 \\
&+\mathrm{m}_k r l_1 \cos(-\theta_1 + \theta_2 + \phi) - m_k r l_4 \cos(-\theta_1 + \theta_2 + \psi + \phi) \\
&+\mathrm{m}_k l_2 l_1 \cos(-\theta_1 + \theta_2) - m_k r l_1 \cos(-\theta_1 + \theta_2) \\
&+\ 2\ \mathrm{m}_k l_1 l_4 \cos(\psi) \\
&+\mathrm{m}_k {l_1}^2 \cos(-\theta_1 + \theta_2)
\end{aligned}
$$

$+\mathrm{m}_k l_1 l_4 \cos(-\theta_1 + \theta_2 + \psi)$
$-\mathrm{m}_k l_4 l_2 \cos(-\theta_1 + \theta_2 + \psi)$
$+\mathrm{m}_k r l_4 \cos(-\theta_1 + \theta_2 + \psi)$
$-\mathrm{m}_k {l_1}^2 - {l_1}^2 - m_k {l_4}^2$

$\mathrm{D}_{13} = -m_h r l_3 \cos(-\theta_1 + \theta_2 + \phi)$
$+\mathrm{m}_h r l_3 \cos(-\theta_1 + \theta_2) - m_h l_2 l_3 \cos(-\theta_1 + \theta_2)$
$-\mathrm{m}_h l_1 l_3 \cos(-\theta_1 + \theta_2) + m_h {l_3}^2 + m_k {l_1}^2 - m_k r l_1 \cos(-\theta_1 + \theta_2)$
$+\mathrm{m}_k r l_4 \cos(-\theta_1 + \theta_2) + m_k l_2 l_1 \cos(-\theta_1 + \theta_2)$
$+\mathrm{m}_k r l_1 \cos(-\theta_1 + \theta_2)$
$-2\ \mathrm{m}_k l_1 l_4 \cos(\psi) - m_k {l_1}^2 \cos(-\theta_1 + \theta_2)$
$+\mathrm{m}_k l_1 l_4 \cos(-\theta_1 + \theta_2 + \psi)$
$+\mathrm{m}_k l_4 l_2 \cos(-\theta_1 + \theta_2 + \psi)$
$-\mathrm{m}_k r l_4 \cos(-\theta_1 + \theta_2 + \psi) + m_k {l_1}^2 + m_k {l_4}^2$

$\mathrm{D}_{14} = m_k r l_4 \cos(-\theta_1 + \theta_2 + \psi + \phi)$
$-\mathrm{m}_k r l_4 \cos(-\theta_1 + \theta_2 + \psi)$
$+\mathrm{m}_k l_4 (l_1 + l_2) \cos(-\theta_1 + \theta_2 + \psi) - m_k l_1 l_4 \cos(\psi)$
$+\mathrm{m}_k {l_4}^2$

$\mathrm{D}_{21} = D_{12}$

$\mathrm{D}_{22} = m_t {l_5}^2 + m_h {l_3}^2 + m_k {l_1}^2 - 2 m_k l_1 l_4 \cos(\psi) + m_k {l_4}^2$

$\mathrm{D}_{23} = -m_h {l_3}^2 - m_k {l_1}^2 + 2 m_k l_1 l_4 \cos(\psi) - m_k {l_4}^2$

$\mathrm{D}_{24} = m_k l_1 l_4 \cos(\psi) - m_k {l_4}^2$

$\mathrm{D}_{31} = D_{13}$

$\mathrm{D}_{32} = D_{23}$

$\mathrm{D}_{33} = m_h {l_3}^2 + m_k {l_1}^2 - 2 l_1 l_4 \cos(\psi) + m_k {l_4}^2$

$\mathrm{D}_{34} = -m_k l_1 l_4 \cos(\psi) + m_k {l_4}^2$

$\mathrm{D}_{41} = D_{14}$

$$\mathrm{D}_{42} = D_{24}$$

$$\mathrm{D}_{43} = D_{34}$$

$$\mathrm{D}_{44} = m_k {l_4}^2$$

$$\begin{aligned}
\mathrm{C}_1 &= 2m_k \sin(\phi)\,\dot{\phi}^2 r - 4m_k \sin(\phi)\,\dot{\phi}^2 l_2 r \\
&\text{-2 } \mathrm{m}_t \sin(\phi)\,\dot{\phi}^2 (l_1 + l_2) r \\
&+2 \ \mathrm{m}_t l_5 \sin(\theta_1 - \phi)\,\dot{\phi}^2 r \\
&\text{-2 } \mathrm{m}_t l_5 \cos(\theta_1 - \phi)\,\dot{\theta}_1 \sin(\phi)\,\dot{\phi} l_1 \\
&+\mathrm{m}_t l_5 \sin(\theta_1 - \phi)\,{\dot{\theta}_1}^2 r \\
&+2 \ \mathrm{m}_t \sin(\phi)\,\dot{\phi}^2 r^2 + 4m_h \sin(\phi)\,\dot{\phi}^2 r^2 \\
&\text{-3 } \mathrm{m}_t l_5 \sin(\theta_1 - \phi)\,\dot{\theta}_1 \dot{\phi} r \\
&+2 \ \mathrm{m}_t l_5 \sin(\theta_1 - \phi)\,\dot{\theta}_1 \dot{\phi} \cos(\phi)\, r \\
&+2 \ \mathrm{m}_h l_3 \sin(\phi)\,\dot{\phi}^2 r \\
&+\mathrm{m}_h l_3 \sin(-\theta_1 + \theta_2 + \phi)\,{\dot{\theta}_1}^2 r \\
&+2 \ \mathrm{m}_h l_3 \cos(-\theta_1 + \theta_2 + \phi)\,\dot{\theta}_2 \sin(\phi)\,\dot{\phi} r \\
&+2 \ \mathrm{m}_h l_3 \cos(-\theta_1 + \theta_2 + \phi)\,\dot{\theta}_1 \dot{\theta}_2 \sin(\phi)\, l_2 \\
&+2 \ \mathrm{m}_h l_3 \cos(-\theta_1 + \theta_2 + \phi)\,\dot{\theta}_1 \dot{\theta}_2 \sin(\phi)\, l_1 \\
&\text{-}\mathrm{m}_h l_3 \cos(-\theta_1 + \theta_2 + \phi)\,{\dot{\theta}_1}^2 \sin(\phi)\, l_2 \\
&+3 \ \mathrm{m}_h l_3 \sin(-\theta_1 + \theta_2 + \phi)\,\dot{\theta}_2 \dot{\phi} r \\
&\text{-}\mathrm{m}_k l_1 \sin(-\theta_1 + \theta_2 + \phi)\,{\dot{\theta}_1}^2 \cos(\phi)\, r \\
&+2 \ \mathrm{m}_k l_1 \sin(-\theta_1 + \theta_2 + \phi)\,\dot{\theta}_1 \dot{\theta}_2 \cos(\phi)\, r \\
&\text{-2 } \mathrm{m}_k {l_1}^2 \sin(-\theta_1 + \theta_2 + \phi)\,\dot{\theta}_1 \dot{\theta}_2 \cos(\phi) \\
&\text{-2 } \mathrm{m}_k l_1 \sin(-\theta_1 + \theta_2 + \phi)\,\dot{\theta}_1 \dot{\theta}_2 \cos(\phi)\, l_2 \\
&\text{-2 } \mathrm{m}_k l_1 \sin(-\theta_1 + \theta_2 + \phi)\,\dot{\theta}_2 \dot{\phi} \cos(\phi)\, r \\
&+2 \ \mathrm{m}_k l_4 \cos(-\theta_1 + \theta_2 + \psi + \phi)\,\dot{\theta}_2 \dot{\psi} \sin(\phi)\, l_2 \\
&\text{- 2 } \mathrm{m}_k l_1 \sin(-\theta_1 + \theta_2 + \phi)\,\dot{\theta}_1 \dot{\phi} \cos(\phi)\, l_2 \\
&\text{- 2 } \mathrm{m}_k {l_1}^2 \sin(-\theta_1 + \theta_2 + \phi)\,\dot{\theta}_1 \dot{\phi} \cos(\phi) \\
&+\mathrm{m}_k {l_1}^2 \sin(-\theta_1 + \theta_2 + \phi)\,{\dot{\theta}_1}^2 \cos(\phi) \\
&+\mathrm{m}_k l_4 \cos(-\theta_1 + \theta_2 + \psi + \phi)\,\dot{\psi}^2 \sin(\phi)\, l_1 \\
&\text{-2 } \mathrm{m}_k l_4 \cos(-\theta_1 + \theta_2 + \psi + \phi)\,\dot{\theta}_2 \dot{\psi} \sin(\phi)\, r \\
&+\mathrm{m}_k l_4 \cos(-\theta_1 + \theta_2 + \psi + \phi)\,{\dot{\theta}_2}^2 \sin(\phi)\, l_1 \\
&+2 \ \mathrm{m}_k l_4 \cos(-\theta_1 + \theta_2 + \psi + \phi)\,\dot{\theta}_2 \dot{\psi} \sin(\phi)\, l_1 \\
&+\mathrm{m}_k l_4 \cos(-\theta_1 + \theta_2 + \psi + \phi)\,{\dot{\theta}_2}^2 \sin(\phi)\, l_2 \\
&\text{-}\mathrm{m}_k l_4 \cos(-\theta_1 + \theta_2 + \psi + \phi)\,\dot{\psi}^2 l_1 \sin(-\theta_1 + \theta_2 + \phi)
\end{aligned}$$

$$
\begin{aligned}
&\text{-m}_k l_4 \cos\left(-\theta_1+\theta_2+\psi+\phi\right) \dot{\theta_2}^2 \sin\left(\phi\right) r \\
&\text{-2 m}_k l_4 \cos\left(-\theta_1+\theta_2+\psi+\phi\right) \dot{\theta_1}\dot{\theta_2} \sin\left(\phi\right) l_1 \\
&+\text{2 l}_4 \cos\left(-\theta_1+\theta_2+\psi+\phi\right) \dot{\theta_1}\dot{\theta_2} \sin\left(\phi\right) r \\
&+\text{2 m}_k l_4 \cos\left(-\theta_1+\theta_2+\psi+\phi\right) \dot{\theta_1}\dot{\psi} \sin\left(\phi\right) r \\
&+\text{2 m}_k {l_1}^2 \cos\left(-\theta_1+\theta_2+\phi\right) \dot{\theta_1}\dot{\theta_2} \sin\left(\phi\right) \\
&\text{-m}_k l_1 \cos\left(-\theta_1+\theta_2+\phi\right) \dot{\theta_1}^2 \sin\left(\phi\right) l_2 \\
&\text{-m}_k {l_1}^2 \cos\left(-\theta_1+\theta_2+\phi\right) \dot{\theta_1}^2 \sin\left(\phi\right) \\
&+\text{m}_k l_1 \cos\left(-\theta_1+\theta_2+\phi\right) \dot{\theta_1}^2 \sin\left(\phi\right) r \\
&+\text{m}_k l_4 \cos\left(-\theta_1+\theta_2+\psi+\phi\right) \dot{\theta_1}^2 \sin\left(\phi\right) l_2 \\
&+\text{2 m}_k l_4 \cos\left(-\theta_1+\theta_2+\psi+\phi\right) \dot{\psi} \sin\left(\phi\right) \dot{\phi} l_2 \\
&\text{-2 m}_k l_4 \cos\left(-\theta_1+\theta_2+\psi+\phi\right) \dot{\theta_1}\dot{\psi} \sin\left(\phi\right) l_1 \\
&\text{-2 l}_1 \cos\left(-\theta_1+\theta_2+\phi\right) \dot{\theta_1}\dot{\theta_2} \sin\left(\phi\right) r \\
&\text{-2 m}_k l_4 \cos\left(-\theta_1+\theta_2+\psi+\phi\right) \dot{\psi} l_1 \sin\left(-\theta_1+\theta_2+\phi\right) \dot{\theta_2} \\
&\text{-2 m}_k l_4 \cos\left(-\theta_2+\psi+\phi\right) \dot{\psi} l_1 \sin\left(-\theta_1+\theta_2+\phi\right) \dot{\phi} \\
&\text{-2 m}_k l_4 \cos\left(-\theta_1+\theta_2+\psi+\phi\right) \dot{\psi} \sin\left(\phi\right) \dot{\phi} r \\
&\text{-m}_k l_4 \cos\left(-\theta_1+\theta_2+\psi+\phi\right) \dot{\theta_1}^2 \sin\left(\phi\right) r \\
&\text{-2 m}_k l_4 \cos\left(-\theta_1+\theta_2+\psi+\phi\right) \dot{\theta_1}\dot{\psi} \sin\left(\phi\right) l_2 \\
&\text{-2 m}_k l_4 \cos\left(-\theta_1+\theta_2+\psi+\phi\right) \dot{\theta_1}\dot{\theta_2} \sin\left(\phi\right) l_2 \\
&\text{-m}_k {l_1}^2 \cos\left(-\theta_1+\theta_2+\phi\right) \dot{\theta_2}^2 \sin\left(\phi\right) \\
&+\text{m}_k l_1 \cos\left(-\theta_1+\theta_2+\phi\right) \dot{\theta_2}^2 \sin\left(\phi\right) r \\
&\text{-m}_h l_3 \sin\left(-\theta_1+\theta_2+\phi\right) \dot{\theta_2}^2 \cos\left(\phi\right) r \\
&\text{-2 m}_h l_3 \sin\left(-\theta_1+\theta_2+\phi\right) \dot{\theta_2}\dot{\phi} \cos\left(\phi\right) r \\
&\text{-m}_k l_1 \cos\left(-\theta_1+\theta_2+\phi\right) \dot{\theta_2}^2 \sin\left(\phi\right) l_2 \\
&+\text{m}_h l_3 \sin\left(-\theta_1+\theta_2+\phi\right) \dot{\theta_2}^2 \cos\left(\phi\right) l_2 \\
&+\text{m}_h l_3 \sin\left(-\theta_1+\theta_2+\phi\right) \dot{\theta_2}^2 \cos\left(\phi\right) r \\
&+\text{ m}_h l_3 \sin\left(-\theta_1+\theta_2+\phi\right) \dot{\theta_1}\dot{\phi} r \\
&+\text{2 m}_h l_3 \sin\left(-\theta_1+\theta_2+\phi\right) \dot{\theta_2}\dot{\phi} \cos\left(\phi\right) l_2 \\
&+\text{m}_h l_3 \sin\left(-\theta_1+\theta_2+\phi\right) \dot{\theta_2}^2 r \\
&\text{-2 m}_k l_1 \cos\left(-\theta_1+\theta_2+\phi\right) \dot{\theta_1} \sin\left(\phi\right) \dot{\phi} r \\
&+\text{2 m}_k l_1 \cos\left(-\theta_1+\theta_2+\phi\right) \dot{\theta_1} \sin\left(\phi\right) \dot{\phi} l_2 \\
&+\text{ 2 m}_k l_1 \cos\left(-\theta_1+\theta_2+\phi\right) \dot{\theta_1}\dot{\theta_2} \sin\left(\phi\right) l_2 \\
&\text{-m}_h l_3 \cos\left(-\theta_1+\theta_2+\phi\right) \dot{\theta_2}^2 \sin\left(\phi\right) l_2 \\
&\text{-m}_h l_3 \cos\left(-\theta_1+\theta_2+\phi\right) \dot{\theta_2}^2 \sin\left(\phi\right) l_1 \\
&\text{- m}_h l_3 \sin\left(-\theta_1+\theta_2+\phi\right) \dot{\theta_1}^2 \cos\left(\phi\right) r \\
&\text{-2 m}_h l_3 \cos\left(-\theta_1+\theta_2+\phi\right) \dot{\theta_1}\dot{\theta_2} \sin\left(\phi\right) r
\end{aligned}
$$

$$
\begin{aligned}
&+\mathrm{m}_h l_3 \cos\left(-\theta_1+\theta_2+\phi\right) \dot{\theta_2}^2 \sin\left(\phi\right) r \\
&\text{-2 } \mathrm{m}_h l_3 \sin\left(-\theta_1+\theta_2+\phi\right) \dot{\theta_1}\dot{\phi} \cos\left(\phi\right) l_1 \\
&\text{- } \mathrm{m}_h l_3 \cos\left(-\theta_1+\theta_2+\phi\right) \dot{\theta_1}^2 \sin\left(\phi\right) l_1 \\
&+2 \mathrm{m}_h l_3 \sin\left(-\theta_1+\theta_2+\phi\right) \dot{\theta_1}\dot{\theta_2} \cos\left(\phi\right) r \\
&+2 \mathrm{m}_h l_3 \sin\left(-\theta_1+\theta_2+\phi\right) \dot{\theta_1}\dot{\phi} \cos\left(\phi\right) r \\
&\text{-2 } \mathrm{m}_h l_3 \sin\left(-\theta_2+\phi\right) \dot{\theta_1}\dot{\phi} \cos\left(\phi\right) l_2 \\
&+\mathrm{m}_h l_3 \sin\left(-\theta_1+\theta_2+\phi\right) \dot{\theta_1}^2 \cos\left(\phi\right) l_2 \\
&+\mathrm{m}_h l_3 \sin\left(-\theta_1+\theta_2+\phi\right) \dot{\theta_1}^2 \cos\left(\phi\right) l_1 \\
&\text{-2 } \mathrm{m}_h l_3 \sin\left(-\theta_1+\theta_2+\phi\right) \dot{\theta_1}\dot{\theta_2} \cos\left(\phi\right) l_2 \\
&+2 \mathrm{m}_h l_3 \cos\left(-\theta_1+\theta_2+\phi\right) \dot{\theta_1} \sin\left(\phi\right) \dot{\phi} l_2 \\
&+2 \mathrm{m}_h l_3 \cos\left(-\theta_1+\theta_2+\phi\right) \dot{\theta_1} \sin\left(\phi\right) \dot{\phi} l_1 \\
&+2 \mathrm{m}_h l_3 \sin\left(-\theta_1+\theta_2+\phi\right) \dot{\theta_2}\dot{\phi} \cos\left(\phi\right) l_1 \\
&\text{-2 } \mathrm{m}_h l_3 \cos\left(-\theta_1+\theta_2+\phi\right) \dot{\theta_2} \sin\left(\phi\right) \dot{\phi} l_1 \\
&\text{-4 } \mathrm{m}_h \sin\left(\phi\right) \dot{\phi}^2 l_2 r \\
&\text{-4 } \mathrm{m}_h \sin\left(\phi\right) \dot{\phi}^2 l_1 r \\
&+2 \mathrm{m}_h l_3 \sin\left(-\theta_1+\theta_2+\phi\right) \dot{\phi}^2 r \\
&\text{-2 } \mathrm{m}_t l_5 \cos\left(\theta_1-\phi\right) \dot{\theta_1} \sin\left(\phi\right) \dot{\phi} l_2 \\
&+\mathrm{m}_t l_5 \cos\left(\theta_1-\phi\right) \dot{\theta_1}^2 \sin\left(\phi\right) l_2 \\
&+\mathrm{m}_t l_5 \cos\left(\theta_1-\phi\right) \dot{\theta_1}^2 \sin\left(\phi\right) l_1 \\
&\text{-}\mathrm{m}_t l_5 \cos\left(\theta_1-\phi\right) \dot{\theta_1}^2 \sin\left(\phi\right) r \\
&+\mathrm{m}_h l_3 \cos\left(-\theta_1+\theta_2+\phi\right) \dot{\theta_1}^2 \sin\left(\phi\right) r \\
&\text{-}\mathrm{m}_t l_5 \sin\left(\theta_1-\phi\right) \dot{\theta_1}^2 \cos\left(\phi\right) r \\
&\text{-2 } \mathrm{m}_t l_5 \sin\left(\theta_1-\phi\right) \dot{\theta_1}\dot{\phi} \cos\left(\phi\right) l_2 \\
&+2 \mathrm{m}_t l_5 \cos\left(\theta_1-\phi\right) \dot{\theta_1} \sin\left(\phi\right) \dot{\phi} r \\
&+\mathrm{m}_t l_5 \sin\left(\theta_1-\phi\right) \dot{\theta_1}^2 \cos\left(\phi\right) l_2 \\
&+\mathrm{m}_t l_5 \sin\left(\theta_1-\phi\right) \dot{\theta_1}^2 \cos\left(\phi\right) l_1 \\
&\text{-2 } \mathrm{m}_t l_5 \sin\left(\theta_1-\phi\right) \dot{\theta_1}\dot{\phi} \cos\left(\phi\right) l_1 \\
&+2 \mathrm{m}_k l_4 \sin\left(-\theta_1+\theta_2+\psi+\phi\right) \dot{\theta_1}\dot{\theta_2} r \\
&\text{-3 } \mathrm{m}_k l_4 \sin\left(-\theta_1+\theta_2+\psi+\phi\right) \dot{\psi}\dot{\phi} r \\
&\text{-}\mathrm{m}_k l_4 \sin\left(-\theta_1+\theta_2+\psi+\phi\right) \dot{\psi}^2 \cos\left(\phi\right) l_2 \\
&+2 \mathrm{m}_k l_4 \sin\left(-\theta_1+\theta_2+\psi+\phi\right) \dot{\theta_1}\dot{\psi} r \\
&\text{-3 } \mathrm{m}_k l_4 \sin\left(-\theta_1+\theta_2+\psi+\phi\right) \dot{\theta_2}\dot{\phi} r \\
&+3 \mathrm{m}_k l_4 \sin\left(-\theta_1+\theta_2+\psi+\phi\right) \dot{\theta_1}\dot{\phi} r \\
&\text{-2 } \mathrm{m}_k l_4 \sin\left(-\theta_1+\theta_2+\psi+\phi\right) \dot{\psi}\dot{\phi} \cos\left(\phi\right) l_2 \\
&\text{-}\mathrm{m}_k l_4 \sin\left(-\theta_1+\theta_2+\psi+\phi\right) \dot{\theta_2}^2 r
\end{aligned}
$$

$$
\begin{aligned}
&\text{-m}_k l_4 \sin\left(-\theta_1+\theta_2+\psi+\phi\right) \dot{\theta_1}^2 r \\
&\text{-2 } \text{m}_k l_4 \cos\left(-\theta_1+\theta_2+\psi+\phi\right) \dot{\theta_1} \sin\left(\phi\right) \dot{\phi} l_2 \\
&\text{-2 } \text{m}_k \sin\left(\phi\right) \dot{\phi}^2 l_1 r \\
&+\text{m}_k l_1 \sin\left(-\theta_1+\theta_2+\phi\right) \dot{\theta_1}^2 r \\
&+2 \text{ m}_k l_1 \sin\left(-\theta_1+\theta_2+\phi\right) \dot{\phi}^2 r \\
&+3 \text{ m}_k l_1 \sin\left(-\theta_1+\theta_2+\phi\right) \dot{\theta}_2 \dot{\phi} r \\
&\text{-2 } \text{m}_k l_1 \sin\left(-\theta_1+\theta_2+\phi\right) \dot{\theta}_1 \dot{\theta}_2 r \\
&\text{-2 } \text{m}_k l_4 \sin\left(-\theta_1+\theta_2+\psi+\phi\right) \dot{\theta}_2 \dot{\phi} \cos\left(\phi\right) l_2 \\
&\text{- 2 } \text{m}_k l_4 \sin\left(-\theta_1+\theta_2+\psi+\phi\right) \dot{\theta}_2 \dot{\phi} \cos\left(\phi\right) l_1 \\
&+2 \text{ m}_k l_4 \sin\left(-\theta_1+\theta_2+\psi+\phi\right) \dot{\psi} \dot{\phi} \cos\left(\phi\right) r \\
&+2 \text{ m}_k l_4 \sin\left(-\theta_1+\theta_2+\psi+\phi\right) \dot{\theta}_2 \dot{\phi} \cos\left(\phi\right) r \\
&+2 \text{ m}_k l_4 \sin\left(-\theta_1+\theta_2+\psi+\phi\right) \dot{\theta}_1 \dot{\psi} \cos\left(\phi\right) l_1 \\
&+ 2 \text{ m}_k l_4 \sin\left(-\theta_1+\theta_2+\psi+\phi\right) \dot{\theta}_2 \dot{\psi} l_1 \cos\left(-\theta_1+\theta_2+\phi\right) \\
&\text{-m}_k l_4 \sin\left(-\theta_1+\theta_2+\psi+\phi\right) \dot{\theta_1}^2 \cos\left(\phi\right) l_2 \\
&\text{-3 } \text{m}_k l_1 \sin\left(-\theta_1+\theta_2+\phi\right) \dot{\theta}_1 \dot{\phi} r \\
&+\text{m}_k l_1 \sin\left(-\theta_1+\theta_2+\phi\right) \dot{\theta_2}^2 r \\
&\text{-m}_k l_4 \sin\left(-\theta_1+\theta_2+\psi+\phi\right) \dot{\theta_1}^2 \cos\left(\phi\right) l_1 \\
&\text{-2 } \text{m}_k l_4 \sin\left(-\theta_1+\theta_2+\psi+\phi\right) \dot{\theta}_2 \dot{\psi} \cos\left(\phi\right) l_2 \\
&\text{-2 } \text{m}_k l_4 \sin\left(-\theta_1+\theta_2+\psi+\phi\right) \dot{\theta}_2 \dot{\psi} \cos\left(\phi\right) l_1 \\
&+\text{m}_k l_4 \sin\left(-\theta_1+\theta_2+\psi+\phi\right) \dot{\theta_2}^2 \cos\left(\phi\right) r \\
&+2 \text{ m}_k l_4 \sin\left(-\theta_1+\theta_2+\psi+\phi\right) \dot{\theta}_2 \dot{\psi} \cos\left(\phi\right) r \\
&\text{-m}_k l_4 \sin\left(-\theta_1+\theta_2+\psi+\phi\right) \dot{\theta_2}^2 \cos\left(\phi\right) l_2 \\
&+4 \text{ m}_k \sin\left(\phi\right) \dot{\phi}^2 r^2 \\
&+2 \text{ m}_k l_4 \sin\left(-\theta_1+\theta_2+\psi+\phi\right) \dot{\theta}_1 \dot{\phi} \cos\left(\phi\right) l_1 \\
&\text{-m}_k l_4 \sin\left(-\theta_1+\theta_2+\psi+\phi\right) \dot{\theta_2}^2 \cos\left(\phi\right) l_1 \\
&+2 \text{ m}_k l_1 \sin\left(-\theta_1+\theta_2+\phi\right) \dot{\theta}_2 \dot{\phi} \cos\left(\phi\right) l_2 \\
&+2 \text{ m}_k {l_1}^2 \sin\left(-\theta_1+\theta_2+\phi\right) \dot{\theta}_2 \dot{\phi} \cos\left(\phi\right) \\
&\text{-2 } \text{m}_k l_4 \sin\left(-\theta_1+\theta_2+\psi+\phi\right) \dot{\phi}^2 r \\
&+2 \text{ m}_k l_4 \sin\left(-\theta_1+\theta_2+\psi+\phi\right) \dot{\theta}_1 \dot{\theta}_2 \cos\left(\phi\right) l_2 \\
&+2 \text{ m}_k l_4 \sin\left(-\theta_1+\theta_2+\psi+\phi\right) \dot{\theta}_1 \dot{\psi} \cos\left(\phi\right) l_2 \\
&\text{-2 } \text{m}_k l_4 \sin\left(-\theta_1+\theta_2+\psi+\phi\right) \dot{\theta}_1 \dot{\theta}_2 \cos\left(\phi\right) r \\
&\text{-2 } \text{m}_k l_4 \sin\left(-\theta_1+\theta_2+\psi+\phi\right) \dot{\theta}_1 \dot{\psi} l_1 \cos\left(-\theta_1+\theta_2+\phi\right) \\
&\text{-2 } \text{m}_k l_4 \sin\left(-\theta_1+\theta_2+\psi+\phi\right) \dot{\theta}_1 \dot{\phi} \cos\left(\phi\right) r \\
&+2 \text{ m}_k l_4 \sin\left(-\theta_1+\theta_2+\psi+\phi\right) \dot{\theta}_1 \dot{\phi} \cos\left(\phi\right) l_2 \\
&+\text{m}_k l_4 \sin\left(-\theta_1+\theta_2+\psi+\phi\right) \dot{\theta_1}^2 \cos\left(\phi\right) r \\
&+\text{m}_k l_1 \sin\left(-\theta_1+\theta_2+\phi\right) \dot{\theta_2}^2 \cos\left(\phi\right) l_2
\end{aligned}
$$

$$
\begin{aligned}
&+2\ \mathrm{m}_k l_4 \sin\left(-\theta_1+\theta_2+\psi+\phi\right)\dot{\theta}_1\dot{\theta}_2\cos\left(\phi\right)l_1\\
&\text{-}\mathrm{m}_k l_1 \sin\left(-\theta_1+\theta_2+\phi\right)r\\
&\text{-}2\ \mathrm{m}_k l_4 \sin\left(-\theta_1+\theta_2+\psi+\phi\right)\dot{\theta}_1\dot{\psi}\cos\left(\phi\right)r\\
&+\mathrm{m}_k {l_1}^2 \sin\left(-\theta_1+\theta_2+\phi\right){\dot{\theta}_2}^2\cos\left(\phi\right)\\
&\text{-}\mathrm{m}_k l_4 \sin\left(-\theta_1+\theta_2+\psi+\phi\right)\dot{\psi}^2 r\\
&\text{-}\mathrm{m}_k l_4 \cos\left(-\theta_1+\theta_2+\psi+\phi\right)\dot{\psi}^2\sin\left(\phi\right)r\\
&+\mathrm{m}_k l_4 \cos\left(-\theta_1+\theta_2+\psi+\phi\right)\dot{\psi}^2\sin\left(\phi\right)l_2\\
&+2\ \mathrm{m}_k l_1 \sin\left(-\theta_1+\theta_2+\phi\right)\dot{\theta}_1\dot{\phi}\cos\left(\phi\right)r\\
&+\mathrm{m}_k l_1 \sin\left(-\theta_1+\theta_2+\phi\right){\dot{\theta}_1}^2\cos\left(\phi\right)l_2\\
&\text{-}2\ \mathrm{m}_k l_4 \cos\left(-\theta_1+\theta_2+\psi+\phi\right)\dot{\theta}_1\sin\left(\phi\right)\dot{\phi}l_1\\
&+2\ \mathrm{m}_k l_4 \cos\left(-\theta_1+\theta_2+\psi+\phi\right)\dot{\psi}\sin\left(\phi\right)\dot{\phi}l_1\\
&+2\ \mathrm{m}_k l_4 \cos\left(-\theta_1+\theta_2+\psi+\phi\right)\dot{\psi}l_1\sin\left(-\theta_1+\theta_2+\phi\right)\dot{\theta}_1\\
&\text{-}2\ \mathrm{m}_h l_3 \cos\left(-\theta_1+\theta_2+\phi\right)\dot{\theta}_2\sin\left(\phi\right)\dot{\phi}l_2\\
&\text{-}2\ \mathrm{m}_h l_3 \cos\left(-\theta_1+\theta_2+\phi\right)\dot{\theta}_1\sin\sin\left(\phi\right)\dot{\phi}r\\
&+2\ \mathrm{m}_k l_4 \cos\left(-\theta_1+\theta_2+\psi+\phi\right)\dot{\theta}_1\sin\left(\phi\right)\dot{\phi}r\\
&+2\ \mathrm{m}_k l_4 \cos\left(-\theta_1+\theta_2+\psi+\phi\right)\dot{\theta}_2\sin\left(\phi\right)\dot{\phi}l_2\\
&+2\ \mathrm{m}_k l_4 \cos\left(-\theta_1+\theta_2+\psi+\phi\right)\dot{\theta}_2\sin\left(\phi\right)\dot{\phi}l_1\\
&\text{-}2\ \mathrm{m}_k l_4 \cos\left(-\theta_1+\theta_2+\psi+\phi\right)\dot{\theta}_2\sin\left(\phi\right)\dot{\phi}r\\
&+2\ \mathrm{m}_k {l_1}^2 \cos\left(-\theta_1+\theta_2+\phi\right)\dot{\theta}_1\sin\left(\phi\right)\dot{\phi}\\
&+\mathrm{m}_k l_4 \sin\left(-\theta_1+\theta_2+\psi+\phi\right)\dot{\psi}^2\cos\left(\phi\right)r\\
&\text{-}2\ \mathrm{m}_k l_4 \sin\left(-\theta_1+\theta_2+\psi+\phi\right)\dot{\psi}\dot{\phi}\cos\left(\phi\right)l_1\\
&+2\ \mathrm{m}_k l_1 \cos\left(-\theta_1+\theta_2+\phi\right)\dot{\theta}_2\sin\left(\phi\right)\dot{\phi}r\\
&\text{-}2\ \mathrm{m}_k {l_1}^2 \cos\left(-\theta_1+\theta_2+\phi\right)\dot{\theta}_2\sin\left(\phi\right)\dot{\phi}\\
&\text{-}2\ \mathrm{m}_k l_4 \sin\left(-\theta_1+\theta_2+\psi+\phi\right)\dot{\theta}_2\dot{\psi}r\\
&+2\ \mathrm{m}_k l_4 \sin\left(-\theta_1+\theta_2+\psi+\phi\right)\dot{\psi}\dot{\phi}l_1\cos\left(-\theta_1+\theta_2+\phi\right)
\end{aligned}
$$

$$
\begin{aligned}
&\mathrm{C}_2 = -m_t l_5 \sin\left(\theta_1-\phi\right)\dot{\phi}^2 r\\
&+\mathrm{m}_t l_5 \cos\left(\theta_1-\phi\right)\dot{\theta}_1\sin\left(\phi\right)\dot{\phi}l_1\\
&+\mathrm{m}_t l_5 \sin\left(\theta_1-\phi\right)\dot{\theta}_1\dot{\phi}r\\
&\text{-}\mathrm{m}_t l_5 \sin\left(\theta_1-\phi\right)\dot{\theta}_1\dot{\phi}\cos\left(\phi\right)r\\
&+\mathrm{m}_k l_1 \sin\left(-\theta_1+\theta_2+\phi\right)\dot{\theta}_2\dot{\phi}\cos\left(\phi\right)r\\
&+\mathrm{m}_k l_1 \sin\left(-\theta_1+\theta_2+\phi\right)\dot{\theta}_1\dot{\phi}\cos\left(\phi\right)l_2\\
&+\ \mathrm{m}_k {l_1}^2 \sin\left(-\theta_1+\theta_2+\phi\right)\dot{\theta}_1\dot{\phi}\cos\left(\phi\right)\\
&+\mathrm{m}_k l_4 \cos\left(-\theta_1+\theta_2+\psi+\phi\right)\dot{\psi}^2 l_1\sin\left(-\theta_1+\theta_2+\phi\right)\\
&\text{-}\mathrm{m}_k l_4 \cos\left(-\theta_1+\theta_2+\psi+\phi\right)\dot{\psi}\sin\left(\phi\right)\dot{\phi}l_2\\
&+2\ \mathrm{m}_k l_4 \cos\left(-\theta_1+\theta_2+\psi+\phi\right)\dot{\psi}l_1\sin\left(-\theta_1+\theta_2+\phi\right)\dot{\theta}_2\\
&+2\ \mathrm{m}_k l_4 \cos\left(-\theta_1+\theta_2+\psi+\phi\right)\dot{\psi}l_1\sin\left(-\theta_1+\theta_2+\phi\right)\dot{\phi}
\end{aligned}
$$

$+\mathrm{m}_k l_4 \cos\left(-\theta_1+\theta_2+\psi+\phi\right)\dot{\psi}\sin\left(\phi\right)\dot{\phi}r$
$+\mathrm{m}_h l_3 \sin\left(-\theta_1+\theta_2+\phi\right)\dot{\theta}_2\dot{\phi}\cos\left(\phi\right)r$
$-\mathrm{m}_h l_3 \sin\left(-\theta_1+\theta_2+\phi\right)\dot{\theta}_2\dot{\phi}\cos\left(\phi\right)l_2$
$-\mathrm{m}_k l_1 \cos\left(-\theta_1+\theta_2+\phi\right)\dot{\theta}_1\sin\left(\phi\right)\dot{\phi}l_2$
$+\ \mathrm{m}_h l_3 \sin\left(-\theta_1+\theta_2+\phi\right)\dot{\theta}_1\dot{\phi}\cos\left(\phi\right)l_1$
$-\ \mathrm{m}_h l_3 \sin\left(-\theta_1+\theta_2+\phi\right)\dot{\theta}_1\dot{\phi}\cos\left(\phi\right)r$
$+\mathrm{m}_h l_3 \sin\left(-\theta_1+\theta_2+\phi\right)\dot{\theta}_1\dot{\phi}\cos\left(\phi\right)l_2$
$-\mathrm{m}_h l_3 \cos\left(-\theta_1+\theta_2+\phi\right)\dot{\theta}_1\sin\left(\phi\right)\dot{\phi}l_2$
$-\mathrm{m}_h l_3 \cos\left(-\theta_1+\theta_2+\phi\right)\dot{\theta}_1\sin\left(\phi\right)\dot{\phi}l_1$
$-\mathrm{m}_h l_3 \sin\left(-\theta_1+\theta_2+\phi\right)\dot{\theta}_2\dot{\phi}\cos\left(\phi\right)l_1$
$+\mathrm{m}_h l_3 \cos\left(-\theta_1+\theta_2+\phi\right)\dot{\theta}_2\sin\dot{\phi}l_1$
$-\mathrm{m}_h l_3 \sin\left(-\theta_1+\theta_2+\phi\right)\dot{\phi}^2 r$
$+\mathrm{m}_t l_5 \cos\left(\theta_1-\phi\right)\dot{\theta}_1\sin\left(\phi\right)\dot{\phi}l_2$
$+\mathrm{m}_t l_5 \sin\left(\theta_1-\phi\right)\dot{\theta}_1\dot{\phi}\cos\left(\phi\right)l_2$
$-\mathrm{m}_t l_5 \cos\left(\theta_1-\phi\right)\dot{\theta}_1\sin\left(\phi\right)\dot{\phi}r$
$+\mathrm{m}_t l_5 \sin\left(\theta_1-\phi\right)\dot{\theta}_1\dot{\phi}\cos\left(\phi\right)l_1$
$+\mathrm{m}_k l_4 \sin\left(-\theta_1+\theta_2+\psi+\phi\right)\dot{\psi}\dot{\phi}r$
$+\mathrm{m}_k l_4 \sin\left(-\theta_1+\theta_2+\psi+\phi\right)\dot{\theta}_2\dot{\phi}r$
$-\mathrm{m}_k l_4 \sin\left(-\theta_1+\theta_2+\psi+\phi\right)\dot{\theta}_1\dot{\phi}r$
$+\mathrm{m}_k l_4 \sin\left(-\theta_1+\theta_2+\psi+\phi\right)\dot{\psi}\dot{\phi}\cos\left(\phi\right)l_2$
$+\mathrm{m}_k l_4 \cos\left(-\theta_1+\theta_2+\psi+\phi\right)\dot{\theta}_1\sin\left(\phi\right)\dot{\phi}l_2$
$-\mathrm{m}_k l_1 \sin\left(-\theta_1+\theta_2+\phi\right)\dot{\phi}^2 r$
$-\mathrm{m}_k l_1 \sin\left(-\theta_1+\theta_2+\phi\right)\dot{\theta}_2\dot{\phi}r$
$-\mathrm{m}_k l_4 \sin\left(-\theta_1+\theta_2+\psi+\phi\right)\dot{\psi}^2 l_1\cos\left(-\theta_1+\theta_2+\phi\right)$
$-\mathrm{m}_k l_4 \sin\left(-\theta_1+\theta_2+\psi+\phi\right)\dot{\psi}\dot{\phi}\cos\left(\phi\right)r$
$-\mathrm{m}_k l_4 \sin\left(-\theta_1+\theta_2+\psi+\phi\right)\dot{\theta}_2\dot{\phi}\cos\left(\phi\right)r$
$-2\ \mathrm{m}_k l_4 \sin\left(-\theta_1+\theta_2+\psi+\phi\right)\dot{\theta}_2\dot{\psi}l_1\cos\left(-\theta_1+\theta_2+\phi\right)$
$+\mathrm{m}_k l_1 \sin\left(-\theta_1+\theta_2+\phi\right)\dot{\theta}_1\dot{\phi}r$
$-\mathrm{m}_k l_4 \sin\left(-\theta_1+\theta_2+\psi+\phi\right)\dot{\theta}_1\dot{\phi}\cos\left(\phi\right)l_1$
$-\mathrm{m}_k l_1 \sin\left(-\theta_1+\theta_2+\phi\right)\dot{\theta}_2\dot{\phi}\cos\left(\phi\right)l_2$
$-\mathrm{m}_k {l_1}^2 \sin\left(-\theta_1+\theta_2+\phi\right)\dot{\theta}_2\dot{\phi}\cos\left(\phi\right)$
$+\mathrm{m}_k l_4 \sin\left(-\theta_1+\theta_2+\psi+\phi\right)\dot{\phi}^2 r$
$+2\ \mathrm{m}_k l_4 \sin\left(-\theta_1+\theta_2+\psi+\phi\right)\dot{\theta}_1\dot{\psi}l_1\cos\left(-\theta_1+\theta_2+\phi\right)$
$+\mathrm{m}_k l_4 \sin\left(-\theta_1+\theta_2+\psi+\phi\right)\dot{\phi}\cos\left(\phi\right)r$
$-\mathrm{m}_k l_4 \sin\left(-\theta_1+\theta_2+\psi+\phi\right)\dot{\theta}_1\dot{\phi}\cos\left(\phi\right)l_2$
$-\mathrm{m}_k l_1 \sin\left(-\theta_1+\theta_2+\phi\right)\dot{\theta}_1\dot{\phi}\cos\left(\phi\right)r$
$+\mathrm{m}_k l_1 \cos\left(-\theta_1+\theta_2+\phi\right)\dot{\theta}_2\sin\left(\phi\right)\dot{\phi}l_2$
$+\mathrm{m}_k l_4 \cos\left(-\theta_2+\psi+\phi\right)\dot{\theta}_1\sin\left(\phi\right)\dot{\phi}l_1$

$$
\begin{aligned}
&\text{-m}_k l_4 \cos\left(-\theta_1+\theta_2+\psi+\phi\right)\left(\phi\right)\dot{\phi} l_1\\
&\text{-2 m}_k l_4 \cos\left(-\theta_1+\theta_2+\psi+\phi\right)\dot{\psi} l_1 \sin\left(-\theta_1+\theta_2+\phi\right)\dot{\theta}_1\\
&+\text{m}_h l_3 \cos\left(-\theta_1+\theta_2+\phi\right)\dot{\theta}_2 \sin\left(\phi\right)\dot{\phi} l_2\\
&+\text{m}_h l_3 \cos\left(-\theta_1+\theta_2+\phi\right)\dot{\theta}_1 \sin\left(\phi\right)\dot{\phi} r\\
&\text{-m}_k l_4 \cos\left(-\theta_1+\theta_2+\psi+\phi\right)\dot{\theta}_1 \sin\left(\phi\right)\dot{\phi} r\\
&\text{-m}_k l_4 \cos\left(-\theta_1+\theta_2+\psi+\phi\phi\right)\dot{\phi} l_1\\
&+\text{m}_k l_4 \cos\left(-\theta_1+\theta_2+\psi+\phi\right)\dot{\theta}_2 \sin\left(\phi\right)\dot{\phi} r\\
&\text{-m}_k {l_1}^2 \cos\left(-\theta_1+\theta_2+\phi\right)\dot{\theta}_1 \sin\left(\phi\right)\dot{\phi}\\
&+\text{m}_k l_4 \sin\left(-\theta_1+\theta_2+\psi+\phi\right)\dot{\psi}\dot{\phi} \cos\left(\phi\right) l_1\\
&\text{-m}_k l_1 \cos\left(-\theta_1+\theta_2+\phi\right)\dot{\theta}_2 \sin\left(\phi\right)\dot{\phi} r\\
&+\text{m}_k {l_1}^2 \cos\left(-\theta_1+\theta_2+\phi\right)\dot{\theta}_2 \sin\left(\phi\right)\dot{\phi}\\
&\text{-2 m}_k l_4 \sin\left(-\theta_1+\theta_2+\psi+\phi\right)\dot{\psi}\dot{\phi} l_1 \cos\left(-\theta_1+\theta_2+\phi\right)
\end{aligned}
$$

$$
\begin{aligned}
&\text{C}_3 = m_h l_3 \cos\left(-\theta_1+\theta_2+\phi\right)\dot{\theta}_2 \sin\left(\phi\right)\dot{\phi} r\\
&+\text{m}_h l_3 \sin\left(-\theta_1+\theta_2+\phi\right)\dot{\theta}_2\dot{\phi} r\\
&\text{-m}_k(-\theta_1+\theta_2+\phi)\,\dot{\phi} \cos\left(\phi\right) r\\
&\text{-m}_k l_1 \sin\left(-\theta_1+\theta_2+\phi\right)\dot{\theta}_1\dot{\phi} \cos\left(\phi\right) l_2\\
&\text{-m}_k {l_1}^2 \sin\left(-\theta_1+\theta_1+\theta_2+\phi\right)\dot{\theta}_1\\
&\text{-m}_k l_4 \cos\left(-\theta_1+\theta_2+\psi+\phi\right)\dot{\psi}^2 l_1 \sin\left(-\theta_1+\theta_2+\phi\right)\\
&\text{-m}_k l_4 \cos\left(-\theta_1+\theta_2+\psi+\phi\right)\dot{\psi} \sin\left(\phi\right)\dot{\phi} r\\
&+\text{m}_h l_3 \sin\left(-\theta_1+\theta_2+\phi\right)\dot{\theta}_2\dot{\phi} \cos\left(\phi\right) l_2\\
&\text{-m}_k l_1 \cos\left(-\theta_1+\theta_2+\phi\right)\dot{\theta}_1 \sin\left(\phi\right)\dot{\phi} r\\
&+\text{m}_k l_1 \cos\left(-\theta_1+\theta_2+\phi\right)\dot{\theta}_1 \sin\left(\phi\right)\dot{\phi} l_2\\
&\text{- m}_h l_3 \sin\left(-\theta_1+\theta_2+\phi\right)\dot{\theta}_1\dot{\phi} \cos\left(\phi\right) l_1\\
&+\text{ m}_h l_3 \sin\left(-\theta_1+\theta_2+\phi\right)\dot{\theta}_1\dot{\phi} \cos\left(\phi\right) r\\
&\text{-m}_h l_3 \sin\left(-\theta_1+\theta_2+\phi\right)\dot{\theta}_1\dot{\phi} \cos\left(\phi\right) l_2\\
&+\text{m}_h l_3 \cos\left(-\theta_1+\theta_2+\phi\right)\dot{\theta}_1 \sin\left(\phi\right)\dot{\phi} l_2\\
&+\text{m}_h l_3 \cos\left(-\theta_1+\theta_2+\phi\right)\dot{\theta}_1 \sin\dot{\phi} l_1\\
&\text{-m}_h l_3 \cos\left(-\theta_1+\theta_2+\phi\right)\dot{\theta}_2 \sin\left(\phi\right)\dot{\phi} l_1\\
&+\text{m}_h l_3 \sin\left(-\theta_1+\theta_2+\phi\right)\dot{\phi}^2 r\\
&\text{-m}_k l_4 \sin\left(-\theta_1+\theta_2+\psi+\phi\right)\dot{\psi}\dot{\phi} r\\
&\text{-m}_k l_4 \sin\left(-\theta_1+\theta_2+\psi+\phi\right)\dot{\theta}_2\dot{\phi} r\\
&+\text{m}_k l_4 \sin\left(-\theta_1+\theta_2+\psi+\phi\right)\dot{\theta}_1\dot{\phi} r\\
&\text{-m}_k l_4 \sin\left(-\theta_2+\psi+\phi\right)\dot{\psi}\dot{\phi} \cos\left(\phi\right) l_2\\
&\text{-m}_k l_4 \cos\left(-\theta_1+\theta_2+\psi+\phi\right)\dot{\theta}_1 \sin\left(\phi\right)\dot{\phi} l_2\\
&+\text{m}_k l_1 \sin\left(-\theta_1+\theta_2+\phi\right)\dot{\phi}^2 r\\
&+\text{m}_k l_1 \sin\left(-\theta_1+\theta_2+\phi\right)\dot{\theta}_2\dot{\phi} r\\
&\text{-m}_k l_4 \sin\left(-\theta_1+\theta_2+\psi+\phi\right)\dot{\theta}_2\dot{\phi} \cos\left(\phi\right) l_2
\end{aligned}
$$

$$
\begin{aligned}
&\text{-m}_k l_4 \sin\left(-\theta_1+\theta_2+\psi+\phi\right)\dot{\theta}_2\dot{\phi}\cos\left(\phi\right)l_1\\
&+\text{m}_k l_4 \sin\left(-\theta_1+\theta_2+\psi+\phi\right)\dot{\psi}\dot{\phi}\cos\left(\phi\right)r\\
&+\text{m}_k l_4 \sin\left(-\theta_1+\theta_2+\psi+\phi\right)\dot{\theta}_2\dot{\phi}\cos\left(\phi\right)r\\
&+2\ \text{m}_k l_4 \sin\left(-\theta_1+\theta_2+\psi+\phi\right)\dot{\theta}_2\dot{\psi}l_1\cos\left(-\theta_1+\theta_2+\phi\right)\\
&\text{-m}_k l_1 \sin\left(-\theta_1+\theta_2+\phi\right)\dot{\theta}_1\dot{\phi}r\\
&+\text{m}_k l_4 \sin\left(-\theta_1+\theta_2+\psi+\phi\right)\dot{\theta}_1\dot{\phi}\cos\left(\phi\right)l_1\\
&+\text{m}_k l_1 \sin\left(-\theta_1+\theta_2+\phi\right)\dot{\theta}_2\dot{\phi}\cos\left(\phi\right)l_2\\
&+\text{m}_k {l_1}^2 \sin\left(-\theta_1+\theta_2+\phi\right)\dot{\theta}_2\dot{\phi}\cos\left(\phi\right)\\
&\text{-m}_k l_4 \sin\left(-\theta_1+\theta_2+\psi+\phi\right)\dot{\phi}^2 r\\
&\text{-2 m}_k l_4 \sin\left(-\theta_1+\theta_2+\psi+\phi\right)\dot{\theta}_1\dot{\psi}l_1\cos\left(-\theta_1+\theta_2+\phi\right)\\
&\text{-m}_k l_4 \sin\left(-\theta_1+\theta_2+\psi+\phi\right)\dot{\phi}\cos\left(\phi\right)r\\
&+\text{m}_k l_4 \sin\left(-\theta_1+\theta_2+\psi+\phi\right)\dot{\theta}_1\dot{\phi}\cos\left(\phi\right)l_2\\
&+\text{m}_k l_1 \sin\left(-\theta_1+\theta_2+\phi\right)\dot{\theta}_1\dot{\phi}\cos\left(\phi\right)r\\
&\text{-m}_k l_1 \cos\left(-\theta_1+\theta_2+\phi\right)\dot{\theta}_2\sin\left(\phi\right)\dot{\phi}l_2\\
&\text{-m}_k l_4 \cos\left(-\theta_1+\theta_2+\psi+\phi\right)\dot{\theta}_1\sin\left(\phi\right)\dot{\phi}l_1\\
&+\text{m}_k l_4 \cos\left(-\theta_1+\theta_2+\psi+\phi\right)\dot{\psi}\sin\left(\phi\right)\dot{\phi}l_1\\
&+2\ \text{m}_k l_4 \cos\left(-\theta_1+\theta_2+\psi+\phi\right)\dot{\psi}l_1\sin\left(-\theta_1+\theta_2+\phi\right)\dot{\theta}_1\\
&\text{-m}_h l_3 \cos\left(-\theta_1+\theta_2+\phi\right)\dot{\theta}_2\sin\left(\phi\right)\dot{\phi}l_2\\
&\text{-m}_h l_3 \cos\left(-\theta_1+\theta_2+\phi\right)\dot{\theta}_1\sin\left(\phi\right)\dot{\phi}r\\
&+\text{m}_k l_4 \cos\left(-\theta_1+\theta_2+\psi+\phi\right)\dot{\theta}_1\sin\left(\phi\right)\dot{\phi}r\\
&+\text{m}_k l_4 \cos\left(-\theta_1+\theta_2+\psi+\phi\right)\dot{\theta}_2\sin\left(\phi\right)\dot{\phi}l_2\\
&+\text{m}_k l_4 \cos\left(-\theta_1+\theta_2+\psi+\phi\right)\dot{\theta}_2\sin\left(\phi\right)\dot{\phi}l_1\\
&\text{-m}_k l_4 \cos\left(-\theta_1+\theta_2+\psi+\phi\right)\dot{\theta}_2\sin\left(\phi\right)\dot{\phi}r\\
&+\text{m}_k {l_1}^2 \cos\left(-\theta_1+\theta_2+\phi\right)\dot{\theta}_1\sin\left(\phi\right)\dot{\phi}\\
&\text{-m}_k l_4 \sin\left(-\theta_1+\theta_2+\psi+\phi\right)\dot{\psi}\dot{\phi}\cos\left(\phi\right)l_1\\
&+\text{m}_k l_1 \cos\left(-\theta_1+\theta_2+\phi\right)\dot{\theta}_2\sin\left(\phi\right)\dot{\phi}r\\
&\text{-m}_k {l_1}^2 \cos\left(-\theta_1+\theta_2+\phi\right)\dot{\theta}_2\sin\left(\phi\right)\dot{\phi}\\
&+2\ \text{m}_k l_4 \sin\left(-\theta_1+\theta_2+\psi+\phi\right)\dot{\psi}\dot{\phi}l_1\cos\left(-\theta_1+\theta_2+\phi\right)
\end{aligned}
$$

$$
\begin{aligned}
&\text{C}_4 = -m_k l_4 \sin\left(-\theta_1+\theta_2+\psi+\phi\right)r\dot{\phi}^2\\
&+\text{m}_k l_4 \cos\left(-\theta_1+\theta_2+\psi+\phi\right)\sin\left(\phi\right)\dot{\phi}l_1\dot{\psi}\\
&+\text{m}_k l_4 \cos\left(-\theta_1+\theta_2+\psi+\phi\right)\sin\left(\phi\right)\dot{\phi}l_2\dot{\psi}\\
&\text{-m}_k l_4 \cos\left(-\theta_1+\theta_2+\psi+\phi\right)\sin\left(\phi\right)\dot{\phi}r\dot{\psi}\\
&\text{- m}_k l_4 \cos\left(-\theta_1+\theta_2+\psi+\phi\right)l_1\sin\left(-\theta_1+\theta_2+\phi\right)\dot{\phi}\dot{\psi}\\
&+\text{m}_k l_4 \cos\left(-\theta_1+\theta_2+\psi+\phi\right)\sin\left(\phi\right)\dot{\phi}r\dot{\theta}_1\\
&+\text{m}_k l_4 \sin\left(-\theta_1+\theta_2+\psi+\phi\right)\cos\left(\phi\right)\dot{\phi}r\dot{\psi}\\
&+\text{m}_k l_4 \cos\left(-\theta_1+\theta_2+\psi+\phi\right)l_1\sin\left(-\theta_1+\theta_2+\phi\right)\dot{\theta}_1\dot{\psi}\\
&\text{-m}_k l_4 \sin\left(-\theta_1+\theta_2+\psi+\phi\right)\cos\left(\phi\right)\dot{\phi}l_1\dot{\psi}
\end{aligned}
$$

$+\mathrm{m}_k l_4 \sin\left(-\theta_1+\theta_2+\psi+\phi\right) l_1 \cos\left(-\theta_1+\theta_2+\phi\right) \dot{\phi}\dot{\psi}$
$-\mathrm{m}_k l_4 \cos\left(-\theta_1+\theta_2+\psi+\phi\right) \sin\left(\phi\right) \dot{\phi} l_2 \dot{\theta}_1$
$-\mathrm{m}_k l_4 \cos\left(-\theta_1+\theta_2+\psi+\phi\right) \sin\left(\phi\right) \dot{\phi} r \dot{\theta}_2$
$+\mathrm{m}_k l_4 \cos\left(-\theta_1+\theta_2+\psi+\phi\right) \sin\left(\phi\right) \dot{\phi} l_1 \dot{\theta}_2$
$-\mathrm{m}_k l_4 \sin\left(-\theta_1+\theta_2+\psi+\phi\right) \cos\left(\phi\right) \dot{\phi} l_2 \dot{\theta}_2$
$+\mathrm{m}_k l_4 \sin\left(-\theta_1+\theta_2+\psi+\phi\right) \cos\left(\phi\right) \dot{\phi} l_2 \dot{\theta}_1$
$+\mathrm{m}_k l_4 \sin\left(-\theta_1+\theta_2+\psi+\phi\right) \cos\left(\phi\right) \dot{\phi} r \dot{\theta}_2$
$-\mathrm{m}_k l_4 \sin\left(-\theta_1+\theta_2+\psi+\phi\right) \cos\left(\phi\right) \dot{\phi} r \dot{\theta}_1$
$-\mathrm{m}_k l_4 \sin\left(-\theta_1+\theta_2+\psi+\phi\right) \cos\left(\phi\right) \dot{\phi} l_1 \dot{\theta}_2$
$-\mathrm{m}_k l_4 \sin\left(-\theta_1+\theta_2+\psi+\phi\right) \cos\left(\phi\right) \dot{\phi} l_2 \dot{\psi}$
$+\mathrm{m}_k l_4 \sin\left(-\theta_1+\theta_2+\psi+\phi\right) \cos\left(\phi\right) \dot{\phi} l_1 \dot{\theta}_1$
$+\mathrm{m}_k l_4 \sin\left(-\theta_1+\theta_2+\psi+\phi\right) r \dot{\phi} \dot{\theta}_1$
$-\mathrm{m}_k l_4 \sin\left(-\theta_1+\theta_2+\psi+\phi\right) r \dot{\phi} \dot{\psi}$
$-\mathrm{m}_k l_4 \sin\left(-\theta_1+\theta_2+\psi+\phi\right) r \dot{\phi} \dot{\theta}_2$
$\mathrm{G}_1 = m_t g \sin\left(\phi\right) r - m_t g \sin\left(\phi\right) l_2$
$-\mathrm{m}_t g \sin\left(\phi\right) l_1 + m_t g l_5 \sin\left(\theta_1-\phi\right)$
$+2\ \mathrm{m}_h g \sin\left(\phi\right) r - 2 m_h g \sin\left(\phi\right) l_2$
$-2\ \mathrm{m}_h g \sin\left(\phi\right) l_1$
$+\mathrm{m}_h g l_3 \sin\left(\phi\right)$
$+\mathrm{m}_h g l_3 \sin\left(-\theta_1+\theta_2+\phi\right)$
$+2\ \mathrm{m}_k g \sin\left(\phi\right) r + m_k g \sin\left(\phi\right) l_4$
$-2\ \mathrm{m}_k g \sin\left(\phi\right) l_2$
$-\mathrm{m}_k g \sin\left(\phi\right) l_1 + m_k g l_1 \sin\left(-\theta_1+\theta_2+\phi\right)$
$-\mathrm{m}_k g l_4 \sin\left(-\theta_1+\theta_2+\psi+\phi\right)$

$\mathrm{G}_2 = -m_t g l_5 \sin\left(\theta_1-\phi\right)$
$-\mathrm{m}_h g l_3 \sin\left(-\theta_1+\theta_2+\phi\right)$
$-\mathrm{m}_k g l_1 \sin\left(-\theta_1+\theta_2+\phi\right)$
$+\mathrm{m}_k g l_4 \sin\left(-\theta_1+\theta_2+\psi+\phi\right)$

$\mathrm{G}_3 = m_h g l_3 \sin\left(-\theta_1+\theta_2+\phi\right)$
$+\mathrm{m}_k g l_1 \sin\left(-\theta_1+\theta_2+\phi\right)$
$-\mathrm{m}_k g l_4 \sin\left(-\theta_1+\theta_2+\psi+\phi\right)$

$\mathrm{G}_4 = -m_k g l_4 \sin\left(-\theta_1+\theta_2+\psi+\phi\right)$